

© 2007

Anne Theresa Tobak

ALL RIGHTS RESERVED

CONSTRUCTION OF THE 3D STRUCTURE OF THE MTOR KINASE-DOMAIN
AND DISCOVERY OF NOVEL MTOR INHIBITORS

by

ANNE THERESA TOBAK

A Dissertation submitted to the

Graduate School-New Brunswick

Rutgers, The State University of New Jersey

in partial fulfillment of the requirements

for the degree of

Doctor of Philosophy

Graduate Program in Computational Biology and Molecular Biophysics

written under the direction of

William Welsh

and approved by

New Brunswick, New Jersey

May, 2007

ABSTRACT OF THE DISSERTATION

Construction of the 3D Structure of the mTOR Kinase-Domain

and Discovery of Novel mTOR Inhibitors

By ANNE THERESA TOBAK

Dissertation Director:

William Welsh

The mammalian target of rapamycin (mTOR) is a serine/threonine kinase involved in the regulation of protein translation and cell proliferation. Based on signals received from nutrition, growth factors, and insulin, mTOR controls cell growth accordingly and is therefore a key target for anticancer therapeutics through its inhibition. Two regions of interest are the FRB domain, where mTOR's natural ligand rapamycin binds when in complex with FKBP12, and the ATP-binding site located within the kinase-domain. Because cancer cells have shown resistance to rapamycin's inhibitory effects, the kinase portion of the protein has become an attractive target for the design of novel inhibitors. Current kinase-domain inhibitors generally lack stability and specificity, mainly due to the absence of a high-resolution crystal structure for mTOR. Therefore, an urgent need exists for more insight into mTOR's three-dimensional (3D) structure as well as improved kinase-domain targeted therapeutics.

The purpose of this study was to construct a 3D structural model of the mTOR kinase-domain using homology modeling techniques, which would then facilitate the discovery of novel compounds with increased inhibitory effects. After constructing the mTOR structural model, we employed pharmaceutical drug design approaches to virtually ‘dock’ known mTOR kinase inhibitors into the putative ligand binding pocket of the kinase domain. Using the key structural features of mTOR inhibitors LY294002 and wortmannin, two pharmacophores were created and later employed as queries in our *in silico* search of commercially available compounds. This systematic procedure yielded 14 novel compounds, 7 from each pharmacophore search, which were purchased in sufficient quantities for initial biological evaluation. Western blot experimental results revealed that 4 of the 14 test compounds show mTOR inhibition *in vitro* at 10uM concentration.

Analysis of the lead compounds’ binding interactions with mTOR identifies several active site residues potentially responsible for ligand binding affinity. In order for a small molecule to possess mTOR inhibitory activity, it must establish interactions with Leu2186, Ile2237, and Ile2356. In addition, it must also make contact with Lys2166 and/or Val2240. Our homology model, in conjunction with these findings, will facilitate the continued rational (computer-aided) design of potent and selective mTOR kinase domain inhibitors.

Acknowledgment

I would like to express my deep and sincere gratitude to my advisor Dr. William Welsh for entrusting me with a fascinating and rewarding research project and for his guidance and encouragement throughout my graduate career.

I would also like to thank the members of my PhD committee for their valuable comments and suggestions: Dr. Wilma Olson, Dr. Paul Ehrlich, Dr. Steven Zheng, and Dr. Tony Kong.

I extend many thanks to all past and present members of the Welsh laboratory for their kindness and support. In particular, I wish to thank Dr. Sonia Arora for her true friendship. Without her guidance and biological expertise, I would not have been able to successfully validate my data experimentally. Special thanks also to Drs. Susan Keenan, Vladyslav Kholodovych, Youyi Peng, Ni Ai, Nina Wang, and Sukjoon Yoon for their assistance, advice, and friendship.

I am grateful to my collaborator Dr. Steven Zheng for approaching Dr. Welsh with this research topic and for allowing me to perform my biological experiments in his laboratory.

I warmly thank Janice Pawlo for her invaluable assistance, cheerfulness, and kindness throughout my time at BioMaPS.

I am grateful to Dr. John Kerrigan for his expertise in molecular dynamics, his friendship, and his generous recommendation letter.

I'd like to thank all of my wonderful friends for keeping laughter in my life. Thank you, Hill, for being my loyal lunch buddy. Thank you, Amy, for your strength, perseverance, and sense of humor. You are a constant inspiration to me. Thank you, Mark, for always believing in me. Your love and friendship has enhanced my life.

I would like to express my loving thanks to Mom and Dad, my sister Rose, and my brother John for their endless encouragement and support.

Most of all, I humbly thank God for being my source of strength through hardships and obstacles, and for blessing me with this accomplishment.

Table of Contents

Abstract	ii
Acknowledgment	iv
Table of Contents	vi
List of Tables	viii
List of Illustrations	ix
Introduction	1
mTOR Function and Mechanism	1
mTOR Structure	3
Rapamycin	4
mTOR Inhibitors	5
PI3K	7
Homology Modeling	9
Structure-Based Design of mTOR Inhibitors	11
Chapter I: mTOR Kinase-Domain Model Construction and the Use of LY294002 Pharmacophore in Discovery of Novel mTOR Inhibitor AT1	12
Materials and Methods	13
Sequence Analysis and Template Selection	13
Homology Modeling	14
Energy Minimization	15
Molecular Dynamics	17
Molecular Docking	19
<i>In Silico</i> Virtual Screening	23
Biological Assays	24
Results and Discussion	26
Sequence Analysis and Template Identification	27
Selection of Final mTOR Kinase-Domain Homology Model	30
Solvated Energy Minimization and Molecular Dynamics Simulation	33
Validation of the mTOR Model	35
mTOR Binding Pocket	37
Binding Pocket Selectivity	40
Virtual Screening	41
Pharmacophore Model	42
Unity Search of mTOR Inhibitors	44
Lipinski's Modified Rule of Five	45
GOLD Docking	45
Biological Assays	48
Docking Simulation Analysis	49
Binding Affinity	49

Selectivity	50
Inhibitor Binding Orientation	53
Summary and Conclusions	60
Chapter II: Wortmannin Pharmacophore in Discovery of Novel mTOR	
Inhibitors AT8, AT9, and AT10	62
Materials and Methods	63
Virtual Screening	63
Biological Assays	64
Results and Discussion	66
Virtual Screening	
Pharmacophore Model	66
UNITY Search of mTOR Inhibitors	67
Lipinski's Modified Rule of Five	67
GOLD Docking	68
Biological Assays	70
Docking Simulation Analysis	71
Binding Affinity	72
Selectivity	73
Inhibitor Binding Orientation	76
Summary and Conclusions	83
Future Work	85
Bibliography	86
Curriculum Vita	95

List of Tables

Table 1: Alignment of the ATP-binding site residues of PI3K and mTOR.

Table 2: Comparison of GOLD scores for Myricetin, Quercetin, and Staurosporine when docked to mTOR and PI3K.

Table 3: Distances (in Angstroms) between LY294002 pharmacophore features.

Table 4: Names, chemical structures, and GOLD scores of the 7 Maybridge test compounds retrieved from LY294002 pharmacophore-based UNITY search.

Table 5: Residues involved in LIGPLOT hydrogen bond and hydrophobic interactions of inhibitors wortmannin, LY294002, LY303511, and AT1 in complex with (A) mTOR model and (B) PI3K γ .

Table 6: Distances (in Angstroms) between wortmannin pharmacophore features.

Table 7: Names, chemical structures, and GOLD scores of the 7 Maybridge test compounds retrieved from wortmannin pharmacophore-based UNITY search.

Table 8: Residues involved in LIGPLOT hydrogen bond and hydrophobic interactions of inhibitors wortmannin, LY294002, LY303511, AT8, AT9, and AT10 in complex with (A) mTOR model and (B) PI3K γ .

List of Illustrations

Fig. 1: Factors impacting mTOR complex.

Fig. 2: mTOR pathway.

Fig. 3: Domains in mTOR. N = N terminus, C = C terminus.

Fig. 4: Chemical structure of rapamycin.

Fig. 5: Chemical structures of mTOR inhibitors A) wortmannin, B) LY294002, C) LY303511, and D) PI-103.

Fig. 6: The crystal structure of PI3K γ (pdb ID=1E7U).

Fig. 7: Energy expression terms in the AMBER force field, including bond-stretching (1), angle-bending (2), torsional (3), van der Waals (4) and electrostatic (5) terms.

Fig. 8: Correlation of experimental binding energy with (a) Chemscore $\Delta G_{binding}$, (b) GOLD score, and (c) GOLD Fitness.

Fig. 9: Sequence alignment of mTOR kinase-domain and PI3K (PDB: 1E7U) kinase-domain with Blastp.

Fig. 10. Structural model of mTOR kinase-domain in complex with ATP.

Fig. 11.a. Carbon backbone Potential Energy (kcal/mol) of mTOR/wortmannin complex is plotted versus MD simulation time (ps).

Fig. 11.b. Carbon backbone RMSD (Angstroms) of mTOR/wortmannin complex is plotted versus MD simulation time (ps).

Fig.12: Ramachandran plot of the final structural model of mTOR.

Fig. 13.a: The final 3D-structural model of the mTOR kinase-domain.

Fig. 13.b: Detailed view of ATP docked within mTOR binding site.

Fig. 14: Pharmacophore inspired by the key structural elements in mTOR inhibitors LY294002 and LY303511.

Fig. 15: Effects of wortmannin, AT1, AT2, and AT3 on phosphorylation of mTOR substrate S6Kinase.

Fig. 16.a: Detailed view of ATP docked within mTOR binding site.

Fig. 16.b: Wortmannin docked within ATP-binding site.

Fig. 16.c: LY294002 docked within mTOR ATP-binding site.

Fig. 16.d: AT1 docked within mTOR ATP-binding site.

Fig. 17.a: Superimposed docked poses of ATP and wortmannin within mTOR ATP-binding site.

Fig. 17.b: Superimposed docked poses of wortmannin and LY294002 within mTOR ATP-binding site.

Fig. 17.c: Superimposed docked poses of ATP and LY294002 within mTOR ATP-binding site.

Fig. 17.d: Superimposed docked poses of ATP and AT1 within mTOR ATP-binding site.

Fig. 18: Pharmacophore inspired by the key structural elements in mTOR inhibitor wortmannin.

Fig. 19: Effects of rapamycin and AT8-AT13 on phosphorylation of mTOR substrate S6Kinase.

Fig. 20a: Detailed view of AT8 docked within mTOR binding site.

Fig. 20b: Detailed view of AT9 docked within mTOR binding site.

Fig. 20c: Detailed view of AT10 docked within mTOR binding site.

Fig. 21.a: Superimposed docked poses of ATP and AT8 within mTOR ATP-binding site.

Fig. 21 b: Superimposed docked poses of wortmannin and AT8 within mTOR ATP-binding site.

Fig. 21 c: Superimposed docked poses of ATP and AT9 within mTOR ATP-binding site.

Fig. 21 d: Superimposed docked poses of wortmannin and AT9 within mTOR ATP-binding site.

Fig. 21 e: Superimposed docked poses of ATP and AT10 within mTOR ATP-binding site.

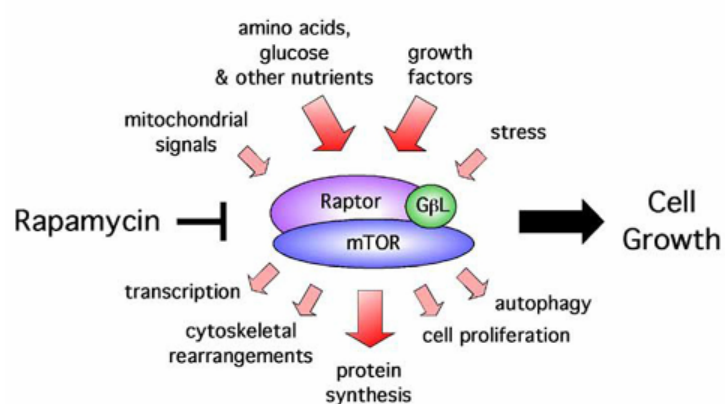
Fig. 21 f: Superimposed docked poses of wortmannin and AT10 within mTOR ATP-binding site.

INTRODUCTION

mTOR Function and Mechanism

The mammalian target of rapamycin (mTOR) is a large 289 kDa (2549 AA) protein expressed ubiquitously in most cells and tissues [1]. Also referred to as FKBP-rapamycin-associated protein (FRAP), mTOR was identified in the mid-1990s as the target of the FKBP12-rapamycin complex [2]. As a crucial protein in PI3K and Akt pathways, mTOR plays a key role in cell growth and proliferation by controlling the rate of protein synthesis. Cofactors of mTOR include Raptor, which binds to mTOR's N-terminus, and GβL, which interacts with mTOR's kinase domain in the C-terminus. While Raptor functions in mediating interactions between mTOR and its substrates, GβL is believed to have relevance in general kinase activity [3].

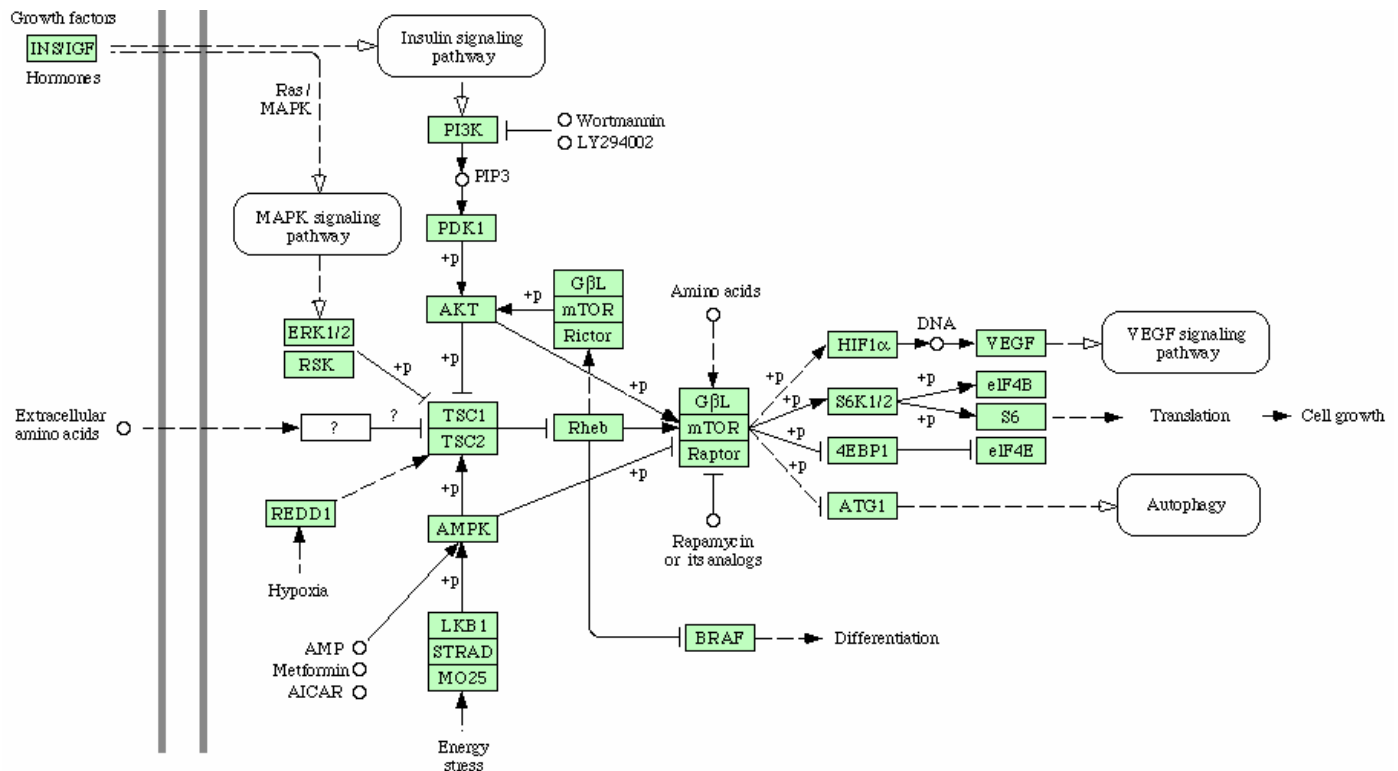
Fig. 1: Factors impacting mTOR complex [4].



Growth factors, nutrients, ATP energy levels, and stress regulate mTOR signaling through their activation of upstream kinases PDK1 and Akt [5]. Activated PDK1 and

Akt phosphorylate mTOR, triggering the phosphorylation of mTOR's endogenous substrates p70/S6 Kinase (p70S6K1) and eIF4E-binding protein (4E-BP1) [5, 6]. The downstream processes affected by this signaling cascade are mRNA translation, ribosomal biosynthesis, amino acid import, macroautophagy, transcription, actin organization, metabolism, cell cycle progression, starvation responses, stress response, and longevity [5, 6]. Therefore, mTOR has clinical implications in several diseases including cancer, hamartoma syndromes, and allograft rejection, as well as autoimmune, cardiovascular, and metabolic disorders [5].

Fig. 2: mTOR pathway [7].



mTOR Structure

Phosphoinositide 3-kinase (PI3K) enzymes generate lipid ‘second messengers’ that mediate signal transduction in the cellular processes of growth, differentiation, survival, proliferation, migration, metabolism, and metastasis [8-14]. Because mTOR’s C terminus is highly homologous to PI3K’s catalytic domain, it is classified as a member of the PIKK family, which is a group of protein kinases that have sequence homology to lipid kinases [15, 16]. mTOR consists of several domains: approximately 20 tandemly repeated HEAT motifs at the N terminus which play a role in protein-protein interactions; the FRB domain (FKBP12-rapamycin binding domain), which mediates the interaction between mTOR and FKBP12-rapamycin complex; the catalytic kinase domain, a 282 residue long PIKK (PI3K-like) kinase domain with protein serine/threonine kinase activity; FAT and FATC domains at the C terminus which modulate catalytic kinase activity; and the putative repressor domain which negatively regulates catalytic activity [17, 18]. From the standpoint of drug discovery, two regions of interest are the FRB domain, where mTOR’s natural ligand rapamycin binds when in complex with FKBP12, and the ATP-binding site located within the kinase domain.

Fig. 3: Domains in mTOR. N = N terminus, C = C terminus.

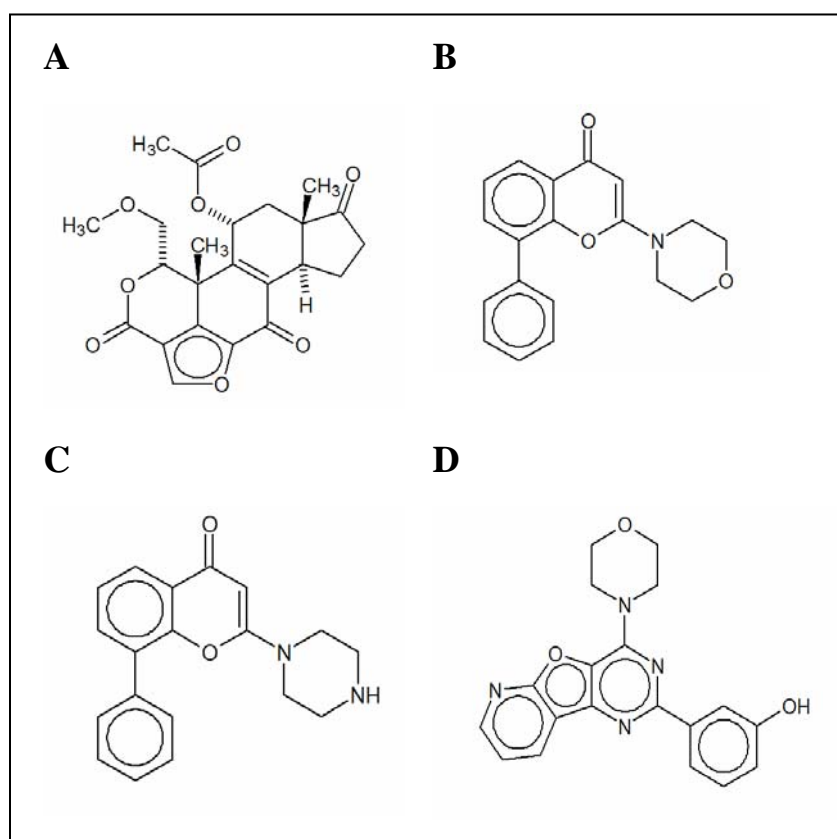


mTOR Inhibitors

Current mTOR kinase inhibitors include wortmannin, LY294002, LY303511, and PI-103. Wortmannin is a steroid-like molecule whose furan ring reacts covalently and thus irreversibly with Lys833 in the ATP-binding site of PI3K's catalytic subunit [32]. This phenomenon is known as suicide inhibition because the protein's active site structure is permanently altered by the incorporation of the inhibitor, rendering the kinase region ineffective. With an IC₅₀ of 0.1-1 μ M for mTOR, wortmannin has shown inhibition of tumor growth in pancreas, lung, and breast cell lines [32-36]. Unlike wortmannin, LY294002 and LY303511 are reversible mTOR inhibitors with 1-30 μ M and 1-100 μ M IC₅₀s, respectively [32]. Unfortunately, there are several disadvantages associated with these three kinase inhibitors. In addition to binding irreversibly to PI3K, wortmannin also inhibits myosin light-chain kinase and thus is not mTOR-specific [37]. Wortmannin's cross-reactivity with PI3K can result in potentially harmful effects. For example, PI3K inhibition could lead to increased insulin insensitivity, thereby posing a risk for the development of diabetes [38]. In addition to its lack of selectivity, wortmannin has been shown to cause hemorrhagic toxicity [39-41]. LY294002 is also nonspecific for mTOR as seen in its inhibition of PI3K and casein kinase-2 [37, 42]. Although LY303511 is mTOR-specific, but its stability has not yet been confirmed in clinical trials. A fourth compound recently discovered is PI-103, which is a PI3K/mTOR dual inhibitor with 0.02-0.083 μ M IC₅₀ for mTOR [43]. The disadvantages of PI-103 as an mTOR inhibitor, however, are its non-selective behavior and the furan ring in its chemical structure. It is possible that PI-103's furan reacts covalently and thus irreversibly with the mTOR active site, as

seen in wortmannin's inhibition. PI-103's strong inhibition could be indicative of covalent interaction between the ligand and protein. Further selectivity and stability studies for PI-103 are underway. The chemical structures for wortmannin, LY294002, LY303511, and PI-103 are shown in Fig. 5.

Fig. 5: Chemical structures of mTOR inhibitors A) wortmannin, B) LY294002, C) LY303511, and D) PI-103.



In general, failure to find improved alternative mTOR kinase domain inhibitors with reversible and mTOR-selective effects is mainly due to the absence of a high-resolution crystal structure for mTOR. Therefore, an urgent need exists for

more insight into mTOR's 3D structure as well as improved kinase domain-targeted therapeutics.

PI3K

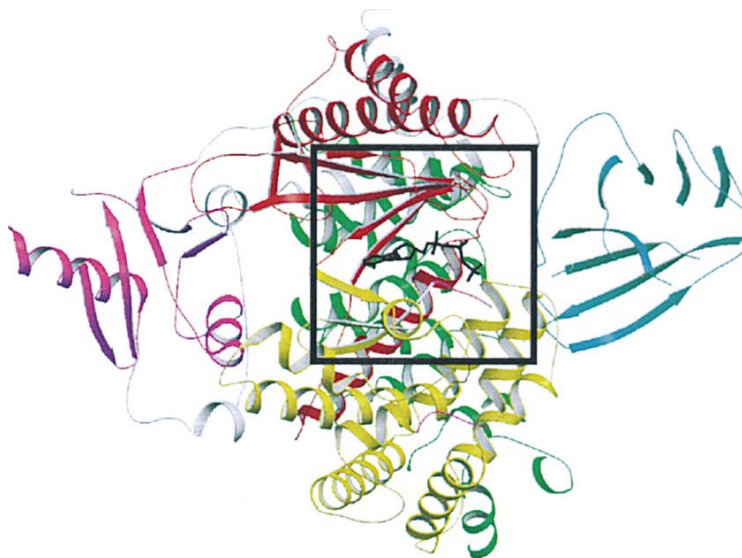
The purpose of this study was to construct a 3D structural model of the mTOR kinase domain using computer-aided homology modeling techniques, which would then facilitate the discovery of novel compounds with increased inhibitory effects. Of the protein crystal structures available in the PDB, *Sus scrofa* phosphatidylinositol 3-kinase (PI3K γ) (PDB ID = 1E7U) had the highest sequence identity (22%) to mTOR's kinase domain and was therefore selected as the template in the model construction [44]. PI3K is a lipid and protein kinase which is instrumental in several intracellular signaling processes such as apoptosis, proliferation, cell motility, and adhesion [44, 45]. The primary function of PI3K is to phosphorylate phosphoinositides at the 3'-OH position of the inositol ring [45]. These phosphoinositides, once phosphorylated, act as membrane tethers for various cellular proteins, such as phospholipid-dependent kinase 1 (PDK1) and protein kinase B (PKB)/Akt, which are critical structures in the mechanisms of diseases such as diabetes, cancer, and chronic inflammation [44, 45].

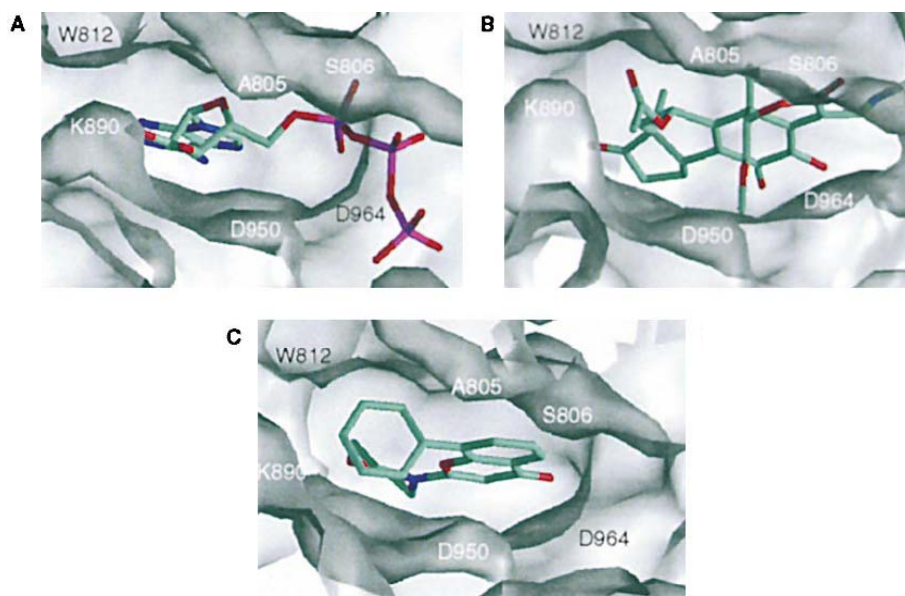
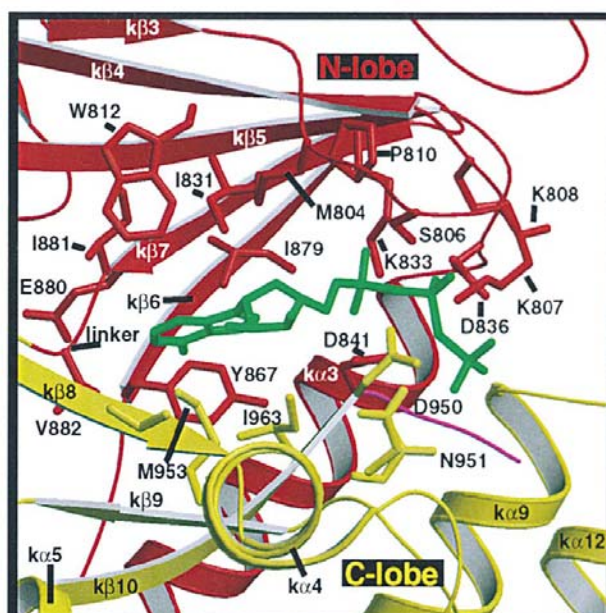
PI3Ks are categorized into three classes based on their secondary structure and substrate specificity [46-48]. Regulatory subunit 101 and catalytic subunit p110 γ classify PI3K γ as the only member of class IB [45]. As seen in Fig. 6, the PI3K catalytic domain is comprised of two regions: an N-terminal region consisting of

a five-stranded β sheet and three α helices and a larger, helical C-terminal region [44]. ATP binds between these two regions of the catalytic domain and, as a result, has many interactions with the residues in the linker between N and C-terminal portions [44].

PI3K γ is a promising target for the treatment of inflammation, thrombosis, allergy, anaphylaxis, rheumatoid arthritis, autoimmunity, lung injury, pancreatitis, heart failure, heart ischaemia, and hypertension [45]. Although mTOR inhibition shares some of these therapeutic uses, it is always advantageous to design target-specific agents for the reduction of potential side-effects.

Fig. 6: The crystal structure of PI3K γ (pdb ID=1E7U) [44]. In the top panel, the protein is displayed by secondary structure and is colored by domain: Ras-binding domain (magenta), C2 domain (cyan), helical domain (green), and catalytic domain with two lobes (N-terminal lobe colored red and C-terminal lobe colored yellow). The middle panel is a detailed view of the ATP-binding site, where ATP (green) is bound to the enzyme and the side chains of active site residues are shown in stick representation. The bottom panel is a zoomed-in view of crystallized A) ATP, B) wortmannin, and C) LY294002 within the ATP-binding site.





Homology Modeling

Homology modeling is the prediction of the secondary and tertiary structure of a disease-relevant protein whose 3D coordinates are unknown and its purpose is to better understand the target protein's binding behavior, mechanism, and function.

The steps required for the creation of a realistic homology model involve the 1) identification of one or more experimentally resolved template structures with high sequence similarity to the target protein, 2) an optimal alignment between the two sequences, and 3) the construction of the model's backbone for residues conserved in the alignment [49]. The coordinates of those regions of the structure that are sequentially different from the template (for example, loops) are generated using *ab initio* techniques. Finally, the homology model is refined with the help of rotamer libraries which optimize each side chain's conformation to an orientation of lowest energy [50].

The quality and accuracy of the homology model is largely dependent on the quality of the pair-wise alignment between the query and template sequences [50]. It is widely accepted that accurate models can be constructed when the identity between target and template sequences exceeds 30%. This is because it has been observed that a model's structural integrity decreases dramatically when sequence identity falls below 30% [50-52].

Our mTOR kinase domain homology model was constructed with Jackal modeling software and was validated with PROCHECK, selectivity docking studies, and secondary structure analysis [53-56].

Structure-Based Design of mTOR Inhibitors

Following the construction and validation of our mTOR kinase-domain model, we employed pharmaceutical drug design approaches to virtually ‘dock’ known mTOR kinase inhibitors into the putative ligand binding pocket of the kinase domain. Analysis of docked interactions enabled us to extract a pharmacophore, i.e., the spatial pattern of common structural features (H-bond acceptors/donors, hydrophobic regions, etc.) that are deemed essential for protein recognition and tight binding. We chose to use the chemical structures of LY294002 and wortmannin as our guides in designing two different pharmacophores. Employing these pharmacophores as queries, we computer-searched our Maybridge database of over 60,000 commercially available compounds for matches. The top-scoring hits emanating from this screening process were computer-docked into the putative ligand binding pocket of the mTOR kinase domain. This systematic procedure yielded a total of 14 novel compounds (7 from each pharmacophore search) which were purchased in sufficient quantities for initial biological evaluation. Of the fourteen test compounds, Western blot inhibitory analysis revealed four with appreciable mTOR inhibitory activity; results were reported as the collection of three independent experiments. At 10 μ M concentration, AT1, AT8, AT9, and AT10 showed significant mTOR inhibition as compared to the control. To our best knowledge, they have not been reported as mTOR inhibitors. Further analysis of mTOR interactions with the test compound revealed several residues responsible for mTOR binding and inhibition.

CHAPTER I:

mTOR KINASE-DOMAIN MODEL
CONSTRUCTION AND THE USE OF LY294002
PHARMACOPHORE IN DISCOVERY OF
NOVEL mTOR INHIBITOR AT1

MATERIALS AND METHODS

Development of the mTOR structural model proceeded in the following steps: sequence analysis and template selection, homology modeling, *in vacuo* and solvated energy minimization (EM), molecular dynamics (MD) simulations, molecular docking, pharmacophore-based *in silico* virtual screening, and biological evaluation. The procedures employed for each step are described below.

Sequence Analysis and Template Selection

All sequence data was obtained from the National Center for Biotechnology Information (NCBI, <http://www.ncbi.nlm.nih.gov/>). The accession numbers for mTOR and template structure PI3K γ are P42345 and O02697, respectively. The mTOR kinase domain sequence, consisting of residues 2153 to 2431, was entered into protein-protein BLAST (blastp, <http://ncbi.nlm.nih.gov/blast>) using PDB db, CD search, and BLOSUM62 search parameters [57]. Multiple sequence alignments for a series of TOR proteins were conducted using ClustalW1.8 routine with default parameters (<http://www.ebi.ac.uk/clustalw/index.html>) [58, 59]. Literature states and multiple sequence alignments confirm that two conserved residues necessary for proper TOR functioning are R2339 and D2357 [60, 61]. The consensus of seven secondary structure predictions (SCRATCH [62], PHD [63], PROF [64], Jpred [65], NNPREP [66], Porter [67], and PSIPRED [68]) was calculated for the mTOR kinase domain.

Homology Modeling

The PI3K γ crystal structure (pdb ID=1E7U) [44] was selected as the template for our mTOR kinase domain structural model. The template structure was obtained from the Research Collaboratory for Structural Bioinformatics Protein Data Bank (<http://www.rcsb.org/pdb>) and submitted to the WHATIF server for structural verification (<http://www.cmbi.kun.nl/gv/servers/WIWWWI/>) [69, 70]. In light of PI3K γ 's somewhat low sequence identity (22%) with mTOR, several models were created using three homology modeling softwares, assorted parameter settings, and several different sequence alignment variations. It was our hope that a larger search space of potential models would increase the likelihood of building a biologically accurate structure. The homology modeling programs used to create the putative models were Jigsaw [71-73], Modeller [49, 74, 75], and Jackal [55] (<http://trantor.bioc.columbia.edu/programs/jackal>) software packages. Following model construction, each model's secondary structure was calculated in Swiss-Pdb Viewer [76], and those models exhibiting disparate secondary structure from the aforementioned consensus prediction were discarded. Also eliminated were models not preserving critical residues R2339 and D2357 and in their alignment with mTOR. From PI3K γ 's crystallized structure (PDB ID=1E7U), wortmannin was extracted, minimized, and docked into the putative ATP-binding sites of our remaining mTOR models. The protein-wortmannin complexes were then subjected to energy minimization for the resolution of any steric clashes.

Energy Minimization

Energy minimization (EM) is the search for minimum points on the potential energy surface of a structure. Objects displace to a position that minimizes their total potential energy and at which the lost energy is released as heat. The arrangements of atoms where energy is minimized correspond to stable states in a system and presumably are biologically more meaningful than atomic arrangements with high energy. The potential energy function is a sum of bonded and non-bonded interaction energies. The former includes bond-stretching, angle-bending, torsional, and occasionally cross energies while the latter includes van der Waals forces and electrostatic energies:

$$E_{\text{pot}} = \sum E_{\text{bond}} + \sum E_{\text{ang}} + \sum E_{\text{tors}} + (\sum E_{\text{cross}}) + \sum E_{\text{vdw}} + \sum E_{\text{electr}}$$

The specific energy expressions in the AMBER force field are listed in Fig. 7. As seen from the equation, the Van der Waals energies are determined by the Lennard-Jones 6-12 function and the electrostatic energies by Coulomb's Law.

Fig. 7: Energy expression terms in the AMBER force field, including bond-stretching (1), angle-bending (2), torsional (3), van der Waals (4) and electrostatic (5) terms [77].

$$\begin{aligned}
 E_{\text{pot}} = & \sum_b K_2(b - b_0)^2 + \sum_{\theta} H_{\theta}(\theta - \theta_0)^2 + \sum_{\phi} \frac{V_n}{2} [1 + \cos(n\phi - \phi_0)] \\
 & (1) \qquad \qquad \qquad (2) \qquad \qquad \qquad (3) \\
 & + \sum \varepsilon [(r^*/r)^{12} - 2(r^*/r)^6] + \sum q_i q_j / \varepsilon_{ij} r_{ij} \\
 & (4) \qquad \qquad \qquad (5)
 \end{aligned}$$

Two gradient methods commonly used in minimization are steepest descents (SD) and conjugate gradient (CG). SD is a very robust method that can effectively minimize systems with unusual or highly restrained geometries by going downhill on the energy surface. It is slow and non-convergent, however, and may not always find a minimum. CG is not as robust, but faster and more efficient, and is always convergent for systems already in fairly low-energy geometries. Therefore, during the refinement of the homology models, SD was initially applied to relieve steric strain and was followed by the more rapid CG method.

For the refinement of the mTOR structural models, two EM protocols were used in the present study: *in vacuo* EM, which was performed prior to virtual docking; and solvated EM with AMBER8 (parm99), thereafter [77, 78]. Models were first subjected to a brief *in vacuo* minimization through a series of independent steps in which the macromolecule hydrogen atoms, side chains, backbone atoms, and ultimately the entire molecule were successively allowed freedom of movement. Using an NVT ensemble, the *in vacuo* system was energy minimized in two phases: first, 50 iterations of constrained SD to relieve bad steric interactions; second, 450 iterations of CG minimization were conducted to more closely approach an energy minimum.

PI3K γ 's ATP-binding site is located between the N and C terminal lobes of the catalytic domain. Because PI3K and mTOR kinase domain inhibitors are ATP-competitive, it is essential that the structural integrity of the ATP-kinase environment be preserved during the refinement process. The wortmannin ligand was extracted

from PI3K γ 's 1E7U structure and docked with GOLD into the preliminary mTOR models. GOLD is a computational tool used for the rapid docking of flexible ligands into protein binding sites (explained in more detail below). Following virtual docking, further refinement of the remaining mTOR-wortmannin complexes was conducted using solvated EM, whereby the models were solvated with a 9 Å radius shell of transferable intermolecular potentials (TIP3) water molecules [79, 80]. The solvated system was energy minimized in two phases: first, 250 iterations of constrained SD and 750 iterations of CG restrained minimization, whereby only the water molecules were free to move to eliminate bad van der Waals contacts; second, 500 iterations of SD and 1000 iterations of CG unrestrained minimization were conducted on the entire system. Following solvated EM, each model system was analyzed. Unstable models with high minimization energy were discarded as they were considered to be biologically unrealistic predictions of mTOR's 3D structure.

Molecular Dynamics

Molecular Dynamics (MD) is a computational technique which generates successive configurations for the atoms in a given system through the integration of Newton's law of motion. MD yields a trajectory that shows how the positions and velocities of the particles in the system vary with time; this trajectory is obtained by solving the differential equation embodied in Newton's second law.

$$\mathbf{F}_i = m_i \mathbf{a}_i$$

$$\frac{d^2 x_i}{dt^2} = \frac{F_{x_i}}{m_i}$$

Where \mathbf{F}_i is the force on the particle i ;

m_i is the mass of the particle;

\mathbf{a}_i is the acceleration of the particle;

\mathbf{x}_i is the position of the particle.

During MD, the relative positions of atoms in a system are relaxed, and their possible conformations in 3D space are explored. Typical uses of MD include searching the conformational space of alternative amino-acid side chains in site-specific mutation studies and identifying likely conformational states for flexible regions of macromolecules such as protein loops.

Following solvated EM, our remaining models were submitted to the MD protocol in AMBER8, using the standard force-field parameter set parm99 [78]. The parameters dielectric constant $\epsilon = 1$ and cutoff distance = 9.0Å were applied for both electrostatic and VdW interactions [78]. The SHAKE algorithm [79] was implemented for bonds involving hydrogen atoms and the time step was set to 2fs. The system was then coupled to a Berendsen bath at 300 K by using a coupling constant $\tau_T = 2\text{ps}$ [81]. The temperature was gradually increased from 100 to 300 K over 20 ps of simulation time with the volume held constant (ensemble NVT). When the system approached 300 K and the density was near 1.0 g/ml, constant pressure (Berendsen algorithm [81]) and temperature controls (NPT) were applied to the system, and the simulation was conducted for 250ps. The pressure of the system was raised to 1atm (ensemble NPT). Trajectory conformations retrieved from the final 200ps (subsequent to system

equilibrium) were averaged and energy minimized once again using 500 iterations of SD and 1000 iterations of CG. Wortmannin was extracted from the averaged structures so that the geometry and stereochemical quality of each minimized model could be examined with WHATIF and PROCHECK [56, 70, 82]. Models receiving poor scores from WHATIF and PROCHECK's structural inspection were discarded.

Molecular Docking

Genetic optimization for ligand docking (GOLD) was chosen to explore ligand conformation in the ATP-binding site of mTOR [83]. GOLD is a ligand-docking application that utilizes a genetic algorithm (GA) to explore not only the full flexibility of the ligand, but also partial flexibility of the protein. Specifically, the OH groups of Ser and Tyr, and the NH_3^+ group of Lys in the active site were allowed to rotate to increase the likelihood of hydrogen-bond formation between the protein and the ligand. Unlike deterministic algorithms, the stochastic nature of GOLD ensures that the search space is well explored and that local energy extremes are less influential in the docking calculation.

GOLD has been fully validated and is highly regarded for its accuracy and reliability [83-86]. GOLD's scoring function, also referred to as GOLD fitness, consists of two intermolecular terms and two intramolecular terms:

$$\text{GOLD Fitness} = S_{hb_ext} + S_{vdw_ext} + S_{hb_int} + S_{vdw_int}$$

Where S_{hb_ext} is the protein-ligand hydrogen bond score;

S_{vdw_ext} is the protein-ligand Van der Waals score;

S_{hb_int} is the score from intramolecular hydrogen bonds in the ligand;

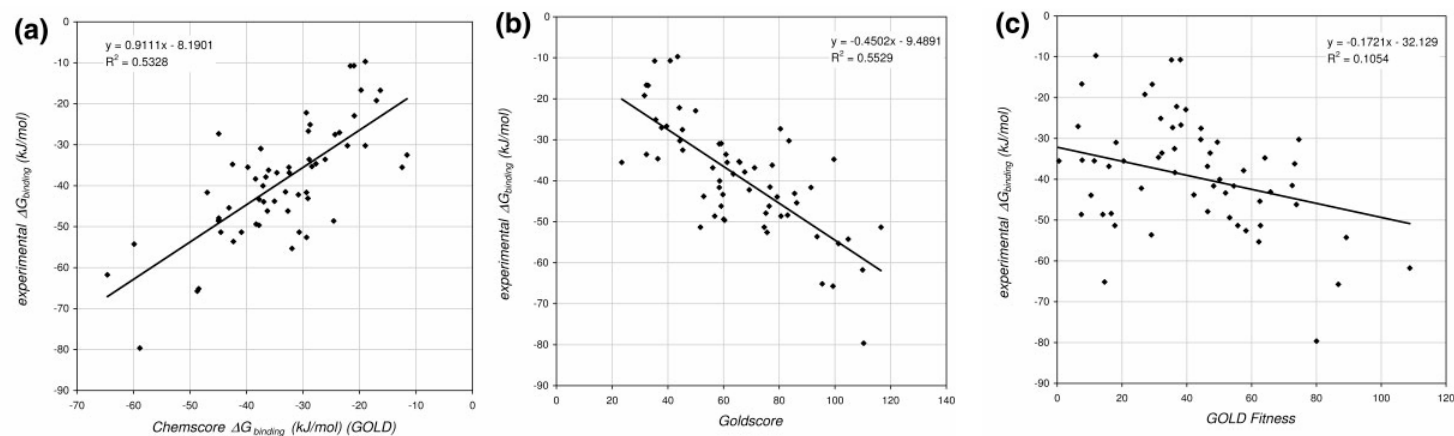
S_{vdw_int} is the score from intramolecular strain in the ligand.

While it produces accurate prediction of ligand binding conformation inside the binding pocket, GOLD fitness was not parameterized against binding affinities ($r^2 = 0.11$ in Fig. 8(c)). Verdonk reported that the modified GOLD scoring function (GOLD fitness minus intra-molecular terms; we refer to it as GOLD score) gave a significantly better correlation with experimental binding affinities ($r^2 = 0.55$ in Fig. 8 (b)), which is comparable to Chemscore's function parameterized against the same experimental binding affinities ($r^2 = 0.53$ in Fig. 8 (a)) [84].

Following the extensive MD simulation of our remaining mTOR models, mTOR inhibitors wortmannin and LY294002 were extracted from PDB crystal structures 1E7U and 1E7V, optimized with MMFF94 force field and atomic charges using Sybyl 7.1 software, and docked with GOLD to the mTOR models [87]. The default algorithm speed was selected, and the number of poses for each inhibitor was set to 10. The ligand binding site was defined as mTOR residues within a 10 Å radius of the centroid of wortmannin's structure docked in PI3Kγ. Early termination was allowed if the RMSD of the top three bound conformations of a ligand were within 0.5 Å. Probabilities for crossover, mutation, and migration were set to 95, 95, and 10,

respectively. The ligand orientation accepted was the top scoring consensus orientation of 10 independent GA runs, each with a maximum number of 10000 GA operations performed on a single population of 100 individuals. The selection pressure was 1.1. After docking, the 10 individual binding poses of each ligand were reranked according to the modified GOLD score. The docking results for each putative model were analyzed, and the model with the highest GOLD scores for wortmannin and LY294002's dockings was selected as the single best structural prediction of mTOR's 3D kinase domain.

Fig. 8: Correlation of experimental binding energy with (a) Chemscore $\Delta G_{binding}$, (b) GOLD score, and (c) GOLD Fitness [84].



***In Silico* Virtual Screening**

Virtual Screening (VS) is becoming increasingly valuable and useful in the field of drug design. Current software enables modelers to rapidly screen large virtual libraries despite the remarkable increase in structural information available for putative drug targets. Also, the more traditional high-throughput synthesis and biological screening methods greatly limit the number and quality of generated hits. In short, VS is fast and inexpensive as it relies solely on computational resources.

There are two types of VS: 1) structure-based VS, requiring knowledge of the target binding site's 3D structure, and 2) ligand-based VS, requiring only one compound with known binding affinity for the target [88]. VS often involves a cascade of different computational techniques including the filtering of drug-like and lead-like properties, molecular docking and scoring, and 3D pharmacophore searching. The goal of VS is to greatly reduce the number of compounds needed for chemical synthesis and biological testing, and ultimately to identify novel chemicals that can be pursued in drug discovery trials. The major disadvantage of VS is the generation of a large number of false positives (inactive compounds with high activity prediction scores) due to energy functions that are not robust enough to reliably rank putative protein-ligand complexes according to their binding affinity [89].

VS techniques were used to screen the Maybridge database for potential mTOR inhibitors. Compounds were analyzed and screened using different criteria, including drug-likeness properties and GOLD score. Our *in silico* structure-based design strategy consisted of the following four steps:

- i) Design a ligand-based pharmacophore model
- ii) Perform a UNITY search of Maybridge compounds
- iii) Use modified Lipinski rules to screen search results
- iv) Dock compounds with GOLD and rank them according to their GOLD score.

Biological Assays

Cell Culture

The human HeLa cervical adenocarcinoma cell line was kindly supplied by Dr. X. F. Steven Zheng of the University of Medicine and Dentistry of New Jersey (Piscataway, New Jersey). HeLa was grown in DMEM, supplemented with 10% fetal bovine serum, 100 units/ml penicillin, and 100 mg/ml streptomycin. Cells were grown to ~60% confluence in 100 mm diameter dishes and maintained in a humidifier incubator at 37° C with 5% CO₂. Cell monolayers were washed in PBS (pH 7.4), scraped into 15-ml conical tubes, and centrifuged at 2500 rpm at 4° C for 5 min. Cell extracts were prepared by homogenizing cell pellets in ice-cold homogenization buffer. The lysates were centrifuged at 13,000 rpm at 4° C for 10 minutes. Protein concentration of the supernatants was determined according to the method of Bradford using a Bio-Rad protein assay kit (Bio-Rad Laboratories, Richmond, CA).

Western Blots

Twenty-five micrograms of cell protein extracts was resolved in 7% SDS-PAGE and transferred to PVDF membrane. Membranes were blocked for 1 hour at room temperature with 5% nonfat dry milk in TBST with 1% Tween 20. Because S6K's

Thr-389 phosphorylation site is mTOR-specific [90], membranes were then incubated overnight at 4° C with Phospho-p70 S6 Kinase (Thr389) primary antibody, as well as p70 S6 Kinase primary antibody (1:1000 dilution in 5% milk/TBST, Cell Signaling Technology, Beverly MA). Following primary incubation, blots were probed with anti-rabbit polyclonal secondary antibody (1:5000 dilution in 5% milk/TBST, Cell Signaling, Beverly MA) the next morning for 1 hour at room temperature before exposing to Western Lightning Western Blot Chemiluminescence Reagent *Plus* (PerkinElmer) per manufacturer's instructions. Blots were scanned by Hewlett Packard Scan Jet, and the intensity of protein bands was quantified by ImageJ software.

RESULTS AND DISCUSSION

Mammalian Target of Rapamycin (mTOR) is involved in the regulation of protein translation and cell proliferation. Therefore, the identification of novel mTOR active compounds, specifically mTOR inhibitors, may elicit numerous pharmacologically beneficial effects as potential treatments for cancer, cardiovascular disease, autoimmunity, and metabolic disorders. Patients have experienced resistance to rapamycin's inhibitory effects and therefore require an alternative to FRB domain-targeted therapeutics. Targeting the kinase domain, rather than the FRB domain, with inhibitors that are more safe, stable, and selective than wortmannin, LY294002, and LY303511 is an attractive and promising strategy.

The success of computational drug design is appreciably improved by the availability of an experimentally resolved target protein. Because no crystallized structure exists for mTOR, the construction of a kinase-domain structural model will facilitate the rational design of clinically significant inhibitors against this biologically-relevant kinase. Along with a novel 3D model of mTOR's kinase domain, we disclose here one compound, AT1, as exhibiting potent mTOR kinase inhibitory activity. This discovery suggests that structural analogs of AT1 might possess even stronger mTOR inhibition and improved bioavailability.

Sequence Analysis and Template Identification

The selection of a template structure is a critical first step in the homology modeling process because it lays the foundation for the future success or failure of the resultant model. Sequence analysis identifies PI3K γ as the crystallized structure in the PDB with the highest sequence identity to the mTOR kinase domain. The monomer of PI3K γ bound to wortmannin (PDB ID = 1E7U) [44] was selected as the template for modeling the mTOR structure because 1E7U has a high 2.0 Å resolution and is in complex with a known mTOR inhibitor. Blastp results revealed 22% identity, 40% similarity, and 22% gaps between the two aligned kinase domain sequences. A WHATIF check of the 1E7U template structure suggested minor structural modifications [70]. Specifically, the only side chain in the active site of 1E7U that needed to be modified was the side chain of His867; WHATIF advised flipping the terminal group 180° so that it may form an energetically more favorable hydrogen bond interaction.

In order to identify functionally conserved regions across the family of TOR kinases, a multiple sequence alignment (MSA) for a series of TOR proteins was conducted using ClustalW1.8 routine with default parameters [58]. The TOR sequences aligned in the MSA were mTOR (P42345), TOR mosquito (Q6JIM3), TOR roundworm (Q95Q95), TOR1 yeast (P35169), TOR2 yeast (P32600), and TOR2 fungus (Q9HFM9). Literature states and the MSA confirmed that two conserved residues necessary for proper TOR1 functioning are R2276 and D2294 [60, 61]. These two residues, when mutated in TOR1 yeast, Arg₂₂₇₆→Pro₂₂₇₆ and Asp₂₂₉₄→Glu₂₂₉₄, disrupt cell cycle

function and cause kinase inactivity [60, 61]. Our MSA results indicate that TOR1 residues R2276 and D2294 correspond to mTOR residues R2339 and D2357, respectively. Other important conserved regions in the TOR family, such as S2035 in mTOR's FRB domain (involved in FKBP12-rapamycin's interaction with mTOR) [92], phosphorylation sites T2446 and S2448 [92], and W2545 (critical residue in C-terminal for proper kinase function) [93] are located outside the kinase domain and are therefore not relevant in our MSA analysis.

The MSA was followed by a pair-wise sequence alignment (PSA) between mTOR and template PI3K γ (Fig. 9). As expected, the two residues essential for TOR kinase activity, R2339 (mTOR)/ R947 (PI3K γ) and D2357 (mTOR)/ D964 (PI3K γ), are well conserved. Examination of the mTOR and PI3K γ aligned sequences also reveals conservation of motifs functionally important in PI3K, and thus potentially important in mTOR. Listed in Table 1 are PI3K residues involved in the binding of ATP and as well as inhibitors wortmannin and LY294002 [37]. Shown in bold, residues V882, M953, and I964 are common to PI3K's interactions with all three small molecules and are aligned with corresponding identical mTOR residues V2240, M2345, and I2356. It is clear that the residues critical for the PI3K binding of ATP, wortmannin, and LY294002 are conserved in their alignment with mTOR.

The alignment scheme shown in Fig. 1 reveals three insertions and three gaps in the mTOR sequence. The insertions are comprised of mTOR residues 2215-2218, 2247-2283, and 2349, whereas the gaps are located between residues 2178-2179, 2294-2295, and 2307-2308. The second insertion is a lengthy 37 residue motif not found in PI3K.

Although MSA analysis reveals that this region is conserved across the entire TOR family, it is completely absent in PI3K. The function of this insertion is unknown, and its structure is difficult to accurately model due to its size. A BLAST search was performed for matches to the 37 residues, but no experimentally determined structures share that same sequence [94]. It is noteworthy to point out the problematic nature of this insertion, as many homology modeling programs are incapable of generating *de novo* coordinates for subsequences longer than 10 residues. As a result, only homology modeling programs capable of generating coordinates for large insertions were utilized in this study.

Particular attention needs to be made in the modeling of inserted residues because there is no structural groundwork provided by the template in these regions. Therefore, in order to glean some insight into the potential structure of these inserted residues, the consensus of seven secondary structure predictions (SCRATCH [62], PHD [63], PROF [64], Jpred [65], NNPREP [66], Porter [67], and PSIPRED [68] algorithms) was calculated for the mTOR kinase domain. The secondary structure consensus will later be used as criteria in selecting a final mTOR structural model.

Fig. 9: Sequence alignment of mTOR kinase-domain and PI3K (PDB: 1E7U) kinase-domain with Blastp [94]. Residues in red are identical, residues in blue are similar, and residues in black are either mismatched or aligned with a gap (represented as a dashed line). The numbers indicate the sequence order in the alignment.

```

mTOR 2161 QVITSKQRPRKLTLMGSN----GHEFVFLKGH-EDLRQDERVMQLFGLV
1E7U 802 KVMASKKKPLWLEFKCADPTALSNETIGIIFKHGDDLQDMLILQILRIM

mTOR 2206 NTLLANDPTSLRKNLISIQRYAVIPLSTNSGLIGWVPHCDTLHALIRDYRE
1E7U 852 ESIWETESL----DLCLLPYGCISTGDKIGMIEIVKDATTI-----

mTOR 2256 KKKILLNIEHRIMLRMAPDYDHLTLMQKVEVFHAVNNT-AGDDLAKLLW
1E7U 889 -----AKIQGSTVGNTGAFKDEVLSHW

mTOR 2305 LKS--PSSEVWFDRRTNYTRSLAVMSMVGYYLGLGDRHPSNIMLDRLSGK
1E7U 911 LKEKCPIEEKQAAVERFVYSCAGYCVATFVLGIGDRHNDNIMISE-TGN

mTOR 2353 ILHIDFG
1E7U 960 LFHIDFG

```

Table 2: Alignment of the ATP-binding site residues of PI3K and mTOR. (10 Å from PI3K/KWT centroid) Numbering represents the amino acid sequence in PI3K. Those PI3K residues shown in red boldface are all involved in PI3K's interactions with ATP, wortmannin, and LY294002. Numbers in the top and bottom rows are the sequence numbers for PI3K and mTOR, respectively.

Seq #	804	806	807	810	812	831	833	867	879	880	881
PI3K	M	S	K	P	W	I	K	Y	I	E	I
mTOR	I	S	K	P	K	L	G	Y	I	G	W
Seq #	2163	2165	2166	2169	2171	2186	2188	2225	2237	2238	2239

882	886	887	950	951	952	953	961	963	964	965
V	T	T	D	N	I	M	F	I	D	F
V	T	T	S	N	L	M	L	I	D	F
2240	2244	2245	2342	2343	2344	2345	2354	2356	2357	2358

Selection of final mTOR kinase-domain homology model

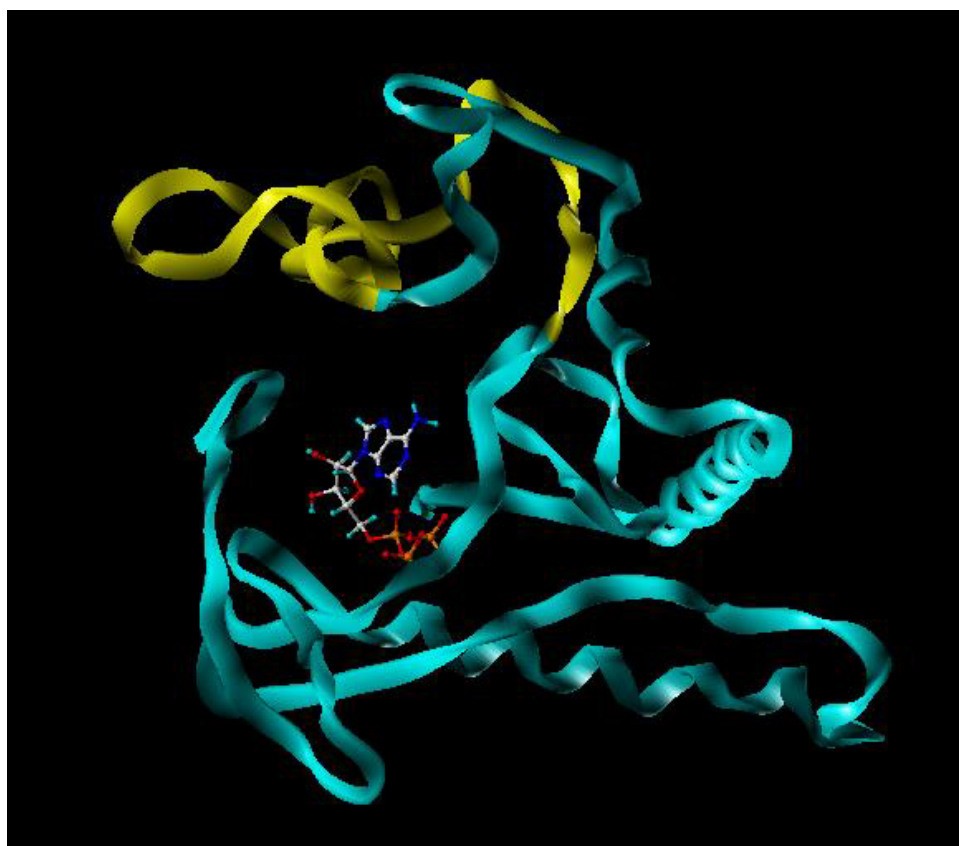
A model's structural integrity decreases dramatically when sequence identity falls below 30% [50, 51]. Therefore, various models of the kinase domain were constructed in an attempt to compensate for PI3K's fairly low sequence identity

(22%) with mTOR. By varying the parameter settings and altering the pair-wise alignments for multiple homology modeling programs (Modeller, Jigsaw, and Jackal) [49, 55, 71-75], many structurally different models were created. Increasing the search space of putative kinase domain structures enabled us to improve our chances of creating a realistic representation of mTOR's active site. In order to decipher the quality of each generated structure, the following elimination criteria were implemented in selecting our final mTOR kinase-domain model: (1) Are PI3K's binding relevant residues conserved in the model? (2) Are residues critical for mTOR kinase activity, i.e. R2339 and D2357, structurally conserved with corresponding PI3K γ residues R947 and D964? (3) Is the model's secondary structure in accord with our secondary structure consensus prediction? (4) Do energy minimization and molecular dynamics simulation of the model result in an unstable structure? (5) Do wortmannin and LY294002 bind well to the model with GOLD docking?

This fifth and last criterion of virtually docking wortmannin and LY294002 to our various mTOR models was implemented for the purpose of studying their protein-ligand interactions. Because literature identifies wortmannin and LY294002 as strong inhibitors of mTOR, those structures exhibiting weak interactions with either compound were discarded, and the model showing docked conformations of wortmannin and LY294002 closest to crystal structure bound conformations was judged to be the most promising. It was the model generated using the NEST module (model building based on a given sequence-template alignment) of Jackal [55], a protein structure-modeling package, that satisfied all 5 requirements and

was selected as our final mTOR kinase-domain model. NEST model building is based on an artificial evolution method, which is used to make residue mutations, insertions, and deletions [95]. For each change, a potential energy function is calculated in which Van der Waals, hydrophobic, electrostatic, torsion angle, and hydrogen bond terms are all contributors, and the change resulting in the most favorable change in energy is accepted [95]. This process is repeated for each residue of the target sequence. A ribbon representation of the final model in complex with ATP is shown in Fig. 2.

Fig. 10: Structural model of mTOR kinase-domain in complex with ATP. The structure's backbone is represented in ribbon form. The 37-residue loop is highlighted in yellow.



Solvated Energy Minimization and Molecular Dynamics Simulation

A more extensive solvated EM and MD simulation of the mTOR model in complex with wortmannin was performed, and the potential energy (PE) and root mean square deviation (RMSD) of backbone atoms were calculated for each sampled conformation, as compared to the starting conformation. Fig. 11a displays the model's potential energy fluctuation throughout the simulation. The increase in PE early in the simulation is explained by the water equilibration phase which takes place during restrained MD in the first 20 ps. Subsequent to water's equilibration, the graph's steady trend toward lower energy conformations is indicative of a stable structure. RMSD plot shown in Fig. 11b illustrates the mTOR system's rapid approach to equilibrium after 50 ps, further supporting the existence of a stable 3D structure.

Representative of a range of equilibrium in the trajectory, an average structure was calculated from a region of stability in our RMSD plot. Conformational snapshots from the trajectory's 50 – 250ps time range were used in the computation. The average structure will later be used for further virtual docking analysis.

Fig. 11.a. Carbon backbone Potential Energy (kcal/mol) of mTOR/wortmannin complex is plotted versus MD simulation time (ps).

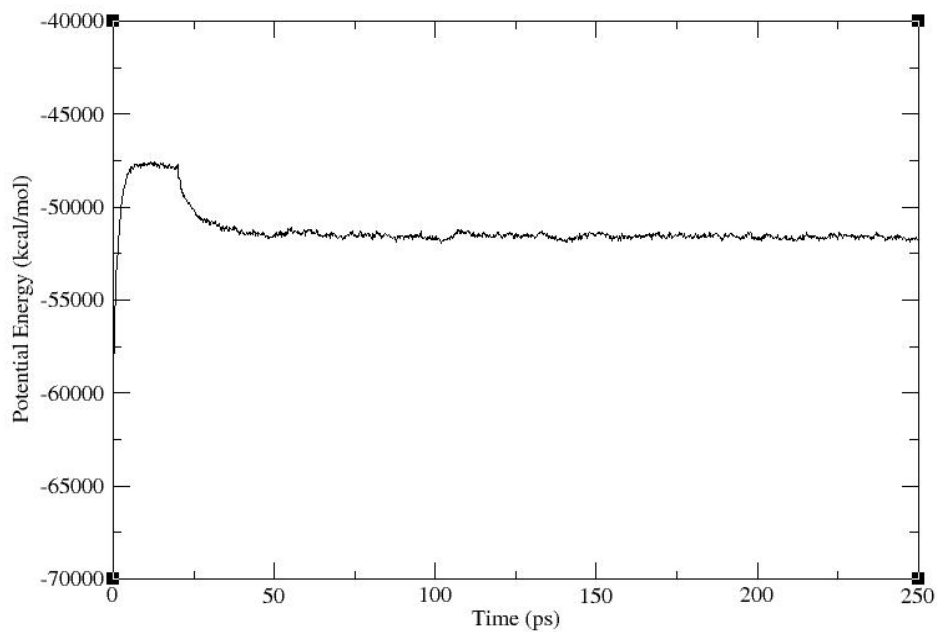
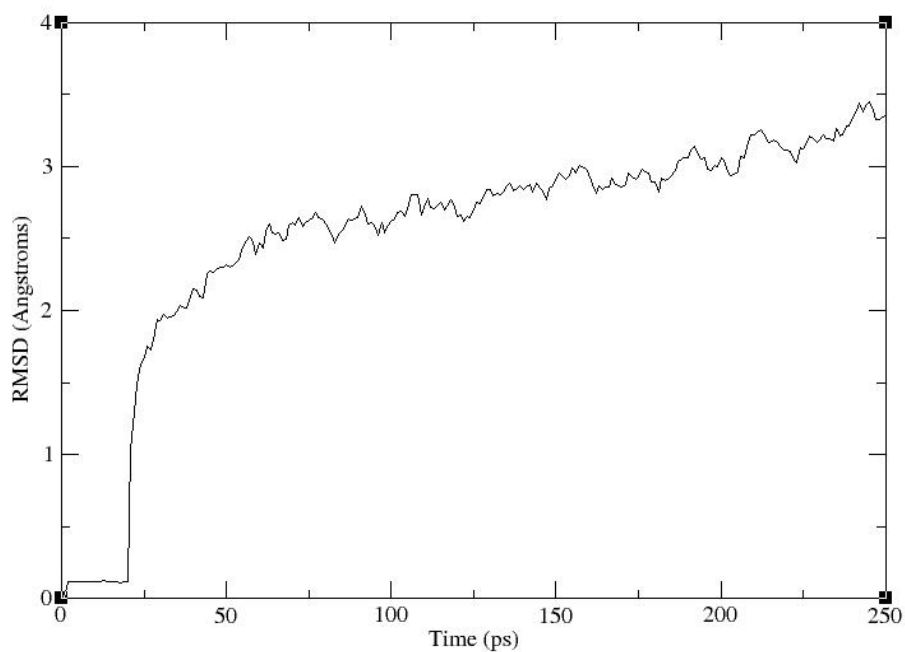


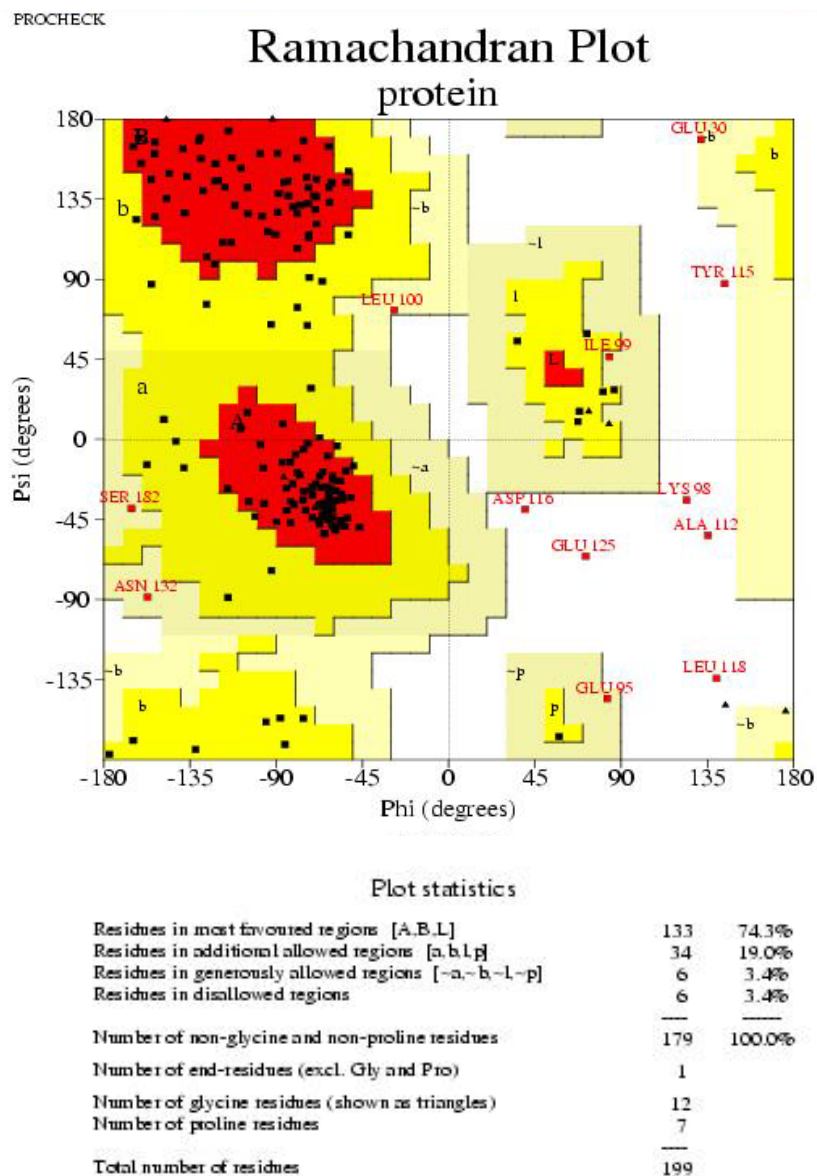
Fig. 11.b. Carbon backbone RMSD (Angstroms) of mTOR/wortmannin complex is plotted versus MD simulation time (ps).



Validation of the mTOR Model

In order to assess the geometrical correctness of the model's backbone phi-psi angles, a Ramachandran plot (Fig. 12) of the energy-minimized structure was produced. PROCHECK results indicate acceptable quality of the structural model with 133 amino acids (74.3%) in the most favored region (A, B, L), 34 amino acids (19%) in the additionally allowed region (a, b, l, p), 6 amino acids (3.4%) in the generously allowed region (~a, ~b, ~l, ~p), and 6 amino acids (3.4%) in the disallowed region. In summary, 96.6% of our model's torsion angles are in favorable positions. Among the six residues in the disallowed region (Lys2258, Ala2272, Tyr2275, Asp2276, Leu2278, and Glu2285), all but Glu2285 are located in the 37 residue loop, which is understandable in light of the difficulty in correctly predicting tertiary structure for a loop of that size. Fortunately, none of 6 residues in the disallowed region are involved in docked interactions with wortmannin, LY294002, or LY303511; this suggests that they are structurally and functionally irrelevant to ligand-binding.

Fig.12: Ramachandran plot of the final structural model of mTOR. In this plot, mTOR residues were numbered 1- 199 for convenience. Therefore Glu30, Glu95, Lys98, Ile99, Leu100, Ala112, Tyr115, Asp116, Leu118, Glu125, Asn132, and Ser182 are equivalent to Glu2190, Glu2255, Lys2258, Ile2259, Leu2260, Ala2272, Tyr2275, Asp2276, Leu2278, Glu2285, Asn2292, and Ser2342, respectively.



Comparison of our secondary structure consensus prediction (calculated prior to model construction) with our model's actual secondary structure, as identified by Swiss-PdbViewer [76] reveals that for 138 out of a total 199 residues (0.69%), our model is consistent with the consensus prediction. When excluding the large 37 residue insertion from the calculation, due to our uncertainty of its structural accuracy, 128 out of 162 residues (0.79%) of the model is consistent with the consensus prediction. Because no residues from the insertion loop take part in ligand binding, we can conclude that the secondary structure of those regions in the model involved in binding affinity and selectivity are ~80% in agreement with prediction.

Interestingly, the docked poses of wortmannin and LY294002 in our final model's active site are almost identical to those of wortmannin and LY294002 when redocked into the active site of PI3K γ (PDB ID=1E7U). This observation suggests that the active site environment was properly maintained when modeling the interior of the ATP-binding pocket.

mTOR Binding Pocket

In general, the binding pocket for mTOR is larger (surface area = 1552.9 Å²; volume = 2451.3 Å³) than that of PI3K (surface area = 746.1 Å²; volume = 1240.9 Å³). This can be explained in part by PI3K amino acids Met804, Ser806, Trp812, Phe832, Lys833, Glu880, Asp950, and Phe961, which correspond to mTOR amino acids Ile2163, Ser2165, Lys2171, Lys2187, Gly2188, Gly2238, Ser2342, and Leu2354, respectively. Met804 has a longer side chain than Ile2163, which crowds the PI3K

pocket. Not only is Ser2165's backbone set farther back in the pocket than that of Ser806, but its side chain is also rotated to the side, thus widening mTOR's binding site. In addition, Trp812, Phe832, Lys833, Glu880, Asp950, and Phe961 are replaced in mTOR by residues with smaller and less bulky side chains. For example, Lys2171 is less bulky than Trp812's indole. Lys2187's side chain is less bulky than Phe832's benzene ring and is oriented in a direction opposite from the center of the binding site in such a way that Lys2187's backbone is closer to the hydrophobic core than its side chain. Lys833 and Glu880 are replaced by glycine residues which lack side chains altogether, thus further increasing the volume of mTOR's active site.

As seen in Sybyl7.1, 21 out of 22 residues (95%) share the same hydrophobicity between mTOR and PI3K. Only residue Trp812 and corresponding Lys2127 have different hydrophobicities; Trp812 is hydrophobic while Lys2127 is hydrophilic. The hydrophobic environment in the model's active site is generally conserved, which is important, since the two proteins share common inhibitors. ATP is shown in complex with a secondary structure representation of our model (Fig. 13a) along with a more detailed view of its interactions with the mTOR active site (Fig. 13b).

Fig. 13.a: The final 3D-structural model of the mTOR kinase domain. The protein is displayed by secondary structure: helix, purple tube; β sheet, yellow arrows; coil, white; turn, cyan. ATP is displayed in CPK (Corey, Pauling, Kulin color scheme).

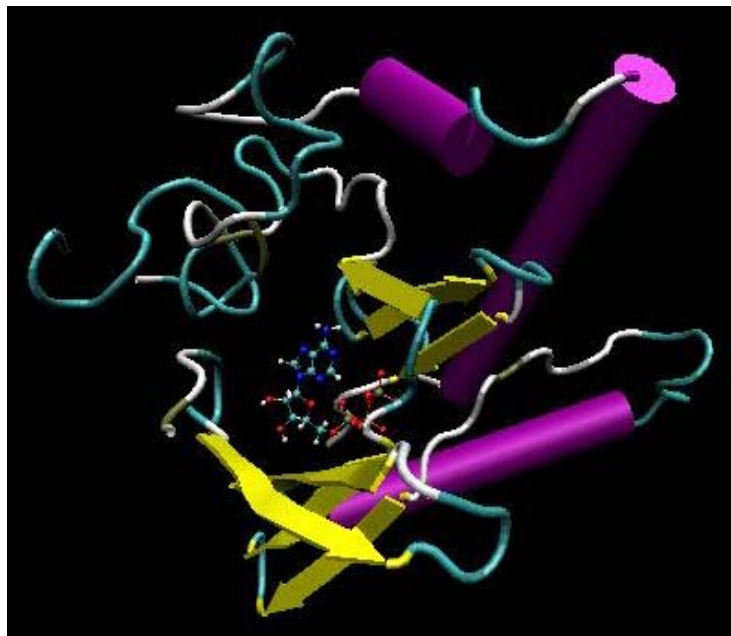
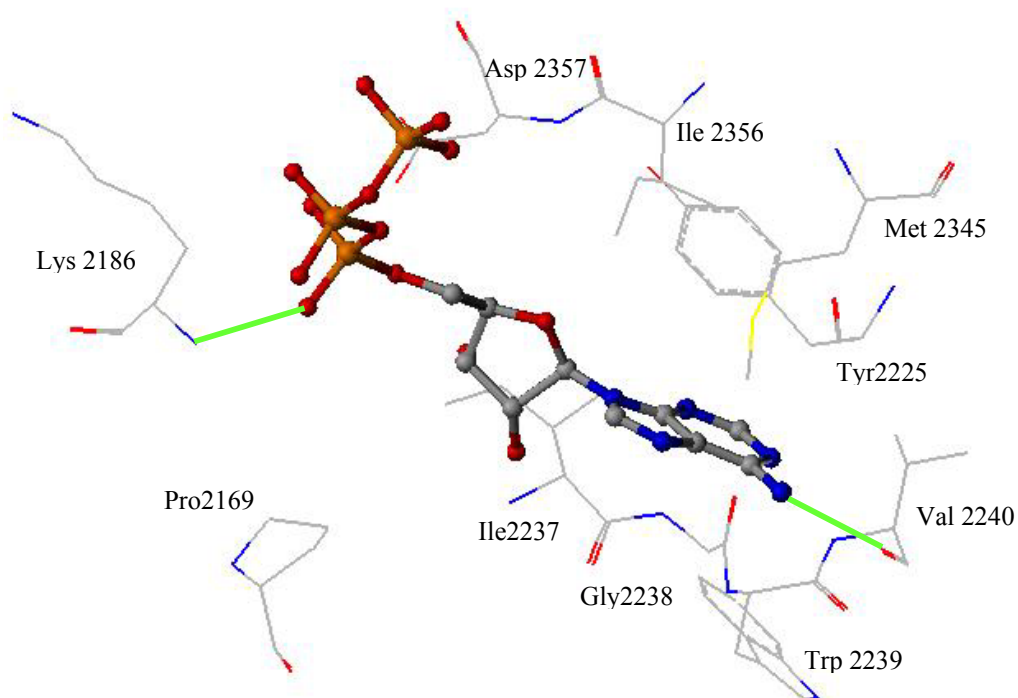


Fig. 13.b: Detailed view of ATP docked within mTOR binding site. ATP is displayed in ball and stick and colored by atom-type, while mTOR residues are displayed in line and colored by atom-type. Hydrogen bonds between ATP and the protein are shown in green.



Binding Pocket Selectivity

At this point, we are confident that mTOR's active site is similar enough to that of PI3K to allow wortmannin and LY294002, which are two known PI3K/mTOR dual inhibitors, to tightly bind to mTOR. Their binding, however, says nothing of the selective nature of mTOR's active site. The true test of our model's selectivity lies in the docking of non-mTOR inhibitors to the structure. Is our model's active site different enough from PI3K to have weak binding with known PI3K inhibitors myricetin, quercetin, and staurosporine [44]? To our knowledge, nothing in literature suggests that myricetin, quercetin, and staurosporine are mTOR inhibitors. In order to investigate mTOR's level of interaction with these three compounds, we docked each of them to our model and to PI3K and compared the GOLD scores. Myricetin, quercetin, and staurosporine were built with Sybyl7.1 and optimized with MMFF94 force field and atomic charges [96, 97]. As described earlier in the Materials and Methods section, the default speed for GOLD was selected, and the number of docked poses for each inhibitor was set to 10. The inhibitor-binding site was defined as 10 Å around the centroid of wortmannin's structure when bound to PI3K γ , and early termination was permitted if the RMSD of the top three conformations was lower than 0.5 Å. The binding conformations were then re-ranked according to GOLD score. As seen in Table 2, myricetin, quercetin, and staurosporine all exhibit stronger binding to PI3K than mTOR. These results suggest that a certain amount of mTOR selectivity has been preserved in our model.

Table 2: Comparison of GOLD scores for Myricetin, Quercetin, and Staurosporine when docked to mTOR and PI3K.

<i>GOLD score</i>	<i>mTOR</i>	<i>PI3K</i>
Myricetin	45.08	64.88
Quercetin	45.27	45.76
Staurosporine	52.18	64.39

Virtual Screening

The application of structure-based VS in the pharmaceutical industry has grown tremendously in recent years. Due in large part to the rapid increase of highly resolved structural information for protein targets, many successful drug discoveries have resulted from the use of high tech compound-searching programs [98, 99]. Clearly, the benefits of gathering 3D structural information without having to invest the time, money, biological expertise, equipment, reagents, and guesswork necessary for traditional high-throughput techniques are invaluable.

With the successful development and validation of our final mTOR model, VS techniques were used to screen the Maybridge database for potential mTOR inhibitors. Compounds were analyzed and screened using different criteria; including pharmacophore feature requirements, drug-likeness properties, and GOLD score. Our *in silico* structure-based design strategy consisted of the following four steps:

- i) Design a ligand-based pharmacophore model
- ii) Perform a UNITY search of Maybridge compounds
- iii) Use modified Lipinski rules to screen search results

- iv) Dock compounds with GOLD and rank them according to their GOLD score.

Pharmacophore Model

A pharmacophore is the spatial pattern of common structural features (H-bond acceptors/donors, hydrophobic regions, etc.) that are deemed essential for protein recognition and tight binding. They are used when searching virtual libraries for new potentially active molecules that share certain spatial and electrostatic properties with known inhibitors.

The pharmacophore used in this study was created based on key structural features found in mTOR inhibitors. The chemical structures of LY294002 and analogue LY303511, rather than wortmannin, was used as our guide in designing the pharmacophore so as to avoid any covalent bond formation. Our pharmacophore (Fig. 14) contains two spherical hydrophobic regions (2.9 Å diameter) and two atom acceptor regions (1.2 Å diameter). Also included are the two fused 6-member rings common to both LY294002 and LY303511. Distances between features are listed in Table 3. A UNITY search of over 60,000 commercially available Maybridge compounds was performed with this pharmacophore using Sybyl7.1.

Fig. 14: Pharmacophore inspired by the key structural elements in mTOR inhibitors LY294002 and LY303511. Hydrophobic regions and acceptor atoms are represented as red and yellow spheres, respectively.

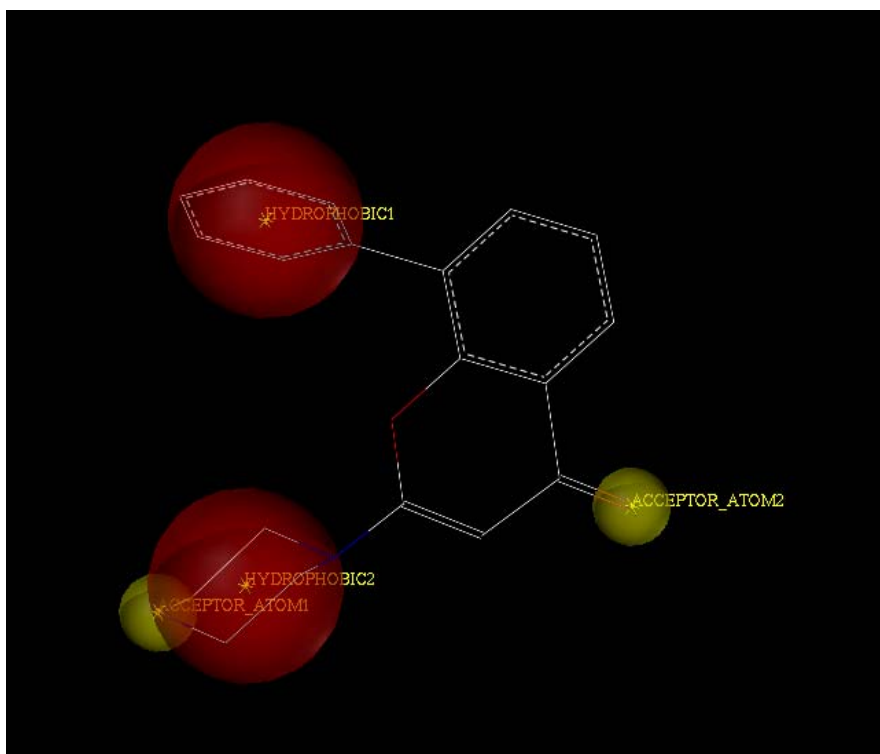


Table 3: Distances (in Angstroms) between pharmacophore features. Centroid coordinates of spheres and rings were used in calculations.

Pharmacophore Feature	Hydrophobic Sphere 1	Hydrophobic Sphere 2	Acceptor Atom 1	Acceptor Atom 2	Aromatic Ring
Hydrophobic Sphere 2	5.992				
Acceptor Atom 1	6.762	1.415			
Acceptor Atom 2	7.410	6.063	7.432		
Aromatic Ring	4.309	6.236	7.561	3.666	
Non-Aromatic Ring	4.937	4.127	5.519	2.667	2.424

UNITY Search of mTOR inhibitors

There are numerous advantages to using virtual libraries in drug discovery. Countless compounds diverse in size, shape, chemical structure, hydrophobicity, and electrostatic property are readily available at a modeler's fingertips. And because these structures are commercially available, they can easily be purchased and biologically tested for inhibitory activity; no chemical synthesis is necessary. This convenience enables researchers to test many more compounds than would be possible if organic synthesis were required. The strategy of purchasing compounds for preliminary biological evaluation and then turning to synthesis later when modifying hits for second-generation commercially unavailable analogues is logical, efficient, and effective.

Employing our LY294002-inspired pharmacophore as a query, we computer-searched our database of over 60,000 commercially available Maybridge compounds for matches. 249 compounds satisfying the pharmacophore's structural criteria were retrieved and their 2D representations were converted into 3D structures by EM. This was performed using the Tripos force field implemented in Sybyl7.1 via the Powell minimization method with simplex initial optimization and a termination gradient of 0.05kcal/(mol* Å). Max iterations were set to 100 with a NB cutoff = 8.0, and a distance dependent dielectric function was used with 1.0 dielectric constant. The 249 energy-minimized compounds were then subjected to Lipinski's modified rule of five.

Lipinski's Modified Rule of Five

Identified by Christopher A. Lipinski in 1997, "Lipinski's rule of five" is a series of features commonly found in orally active drugs [100]. These features are widely used as general criteria when predicting the drug-likeness, or oral bioactivity, of a molecule. From the Maybridge database, the LY294002 pharmacophore search yielded 249 compounds, which were then filtered down in number through the use of Lipinski's "rule of 5" (shown below in bold) and other drug-likeness criteria [100]:

- 1) **Molecular weight < 500**
- 2) **CLogP < 5**
- 3) **Hydrogen bond acceptors > 10**
- 4) **Hydrogen bond donors < 5**
- 5) Rotatable bonds < 10
- 6) Rotatable Nitrogens < 10

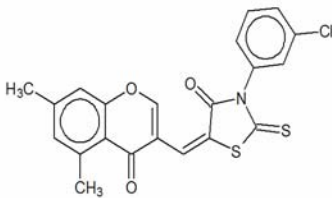
Specifically, compounds were discarded if their molecular weight ≥ 500 , their clogP ≥ 5.0 , their Hbond donors ≥ 5 , their Hbond acceptors ≥ 10 , their rotatable bonds ≥ 10 , or their rotatable Nitrogens ≥ 10 .

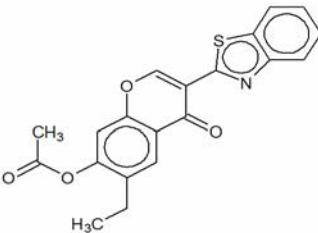
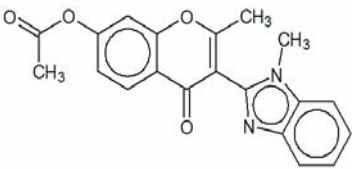
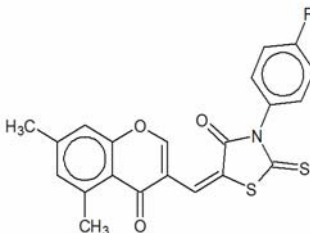
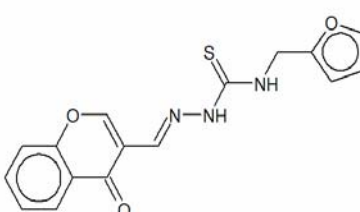
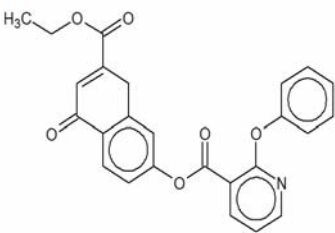
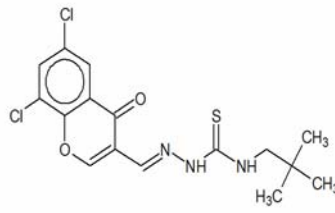
GOLD Docking

Those compounds satisfying Lipinski's modified rule of 5 were then docked to our homology model with GOLD. Default parameters for docking speed were assigned and the number of docked poses for each ligand was set to 10. The binding site was defined as 10 Å around the centroid of wortmannin's structure when docked to PI3K γ ,

and early termination was allowed if the RMSD of the top three docked orientations was lower than 0.5 Å. A modified GOLD scoring function (GOLD fitness minus intra-molecular terms, resulting in a GOLD score) for each compound was calculated. This modification was made because, although GOLD fitness accurately predicts the ligand binding conformation inside the binding pocket, it poorly correlates with experimental binding affinity ($r^2 = 0.11$) [84]. GOLD score's reported correlation with experimental data, however, is considerably greater ($r^2 = 0.55$) [84]. The compounds' GOLD scores were calculated, the docked orientations were resorted based on GOLD score instead of GOLD fitness, and the top-ranking seven compounds predicted to have the highest binding affinity for mTOR were selected for further biological evaluation. The Maybridge identification numbers of the seven compounds RF00683, JFD02982, JFD02983, RF00684, RF00105, RH00411, and RF01260 were renamed AT1-AT7 for convenience. The chemical structures and GOLD scores of the seven test compounds are shown in Table 4.

Table 4: Names, chemical structures, and GOLD scores of the 7 test compounds (Maybridge) retrieved from pharmacophore-based UNITY search.

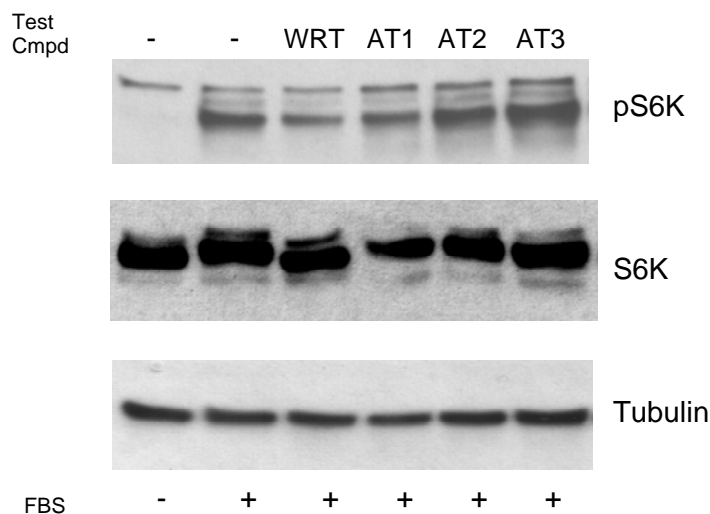
Name	Structure	gold score
RF_00683 (AT1)		54.18

JFD_02982 (AT2)		52.20
JFD_02983 (AT3)		51.49
RF_00684 (AT4)		51.18
RF_00105 (AT5)		49.74
RH_00411 (AT6)		49.67
RF_01260 (AT7)		48.30

Biological Assays

For the validation of our model and its contribution to our search for novel inhibitors, Western blot experiments were used to screen our seven top-ranking compounds AT1-AT7 obtained by *in silico* VS. The seven compounds were purchased from the Maybridge, and their inhibitory activity on mTOR was biologically evaluated in collaboration with Dr. X. F. Steven Zheng's laboratory (UMDNJ). Experimental results show that the compound predicted to have the highest binding affinity for mTOR, AT1, does indeed inhibit mTOR at 10 μ M concentration when compared to the wortmannin (WRT) control (Fig 15). Results were reported as the collection of three independent experiments in duplicate. AT1 represents a potential drug candidate for a wide range of pharmacological applications including therapeutic agents for treatment of cancer, cardiovascular disease, autoimmunity, and metabolic disorders. Experimental IC₅₀ and selectivity studies for AT1 are currently underway.

Fig. 15: Effects of wortmannin, AT1, AT2, and AT3 on phosphorylation of mTOR substrate S6Kinase. Data for AT4-AT7 not shown. HeLa cells were treated with wortmannin for 30 min and AT1, AT2, AT3 for 6hrs. Cell extracts were prepared and run by 7.5% SDS-PAGE, followed by Western blot analysis using anti-pS6Kinase, anti-S6Kinase, and anti-Tubulin antibodies. Representative of three experiments.



Docking Simulation Analysis

Once AT1's inhibition of mTOR was confirmed *in vitro*, GOLD docking results from the prior virtual screening were revisited for a more thorough analysis of its binding interactions inside the mTOR kinase bonding pocket. Our primary objective was to examine mTOR's interaction with AT1 and in doing so identify residues responsible for binding, glean insights regarding selectivity, and increase our understanding of inhibitor orientations when bound to the active site.

The subtleties of mTOR binding cannot be fully understood simply from the analysis of AT1's interaction within the binding pocket. The protein's interface with other known inhibitors must also be explored. As a means of comparison, the binding behavior of PI3K's crystallized complexes was investigated as well. 2D LIGPLOT diagrams were created as representations of mTOR's active site in complex with ATP, wortmannin, LY294002, LY303511, and AT1, as well as PI3K's active site in complex with ATP, wortmannin, LY294002, quercetin, myricetin, and staurosporine [101].

Binding affinity

Analysis of the mTOR model's interactions with docked inhibitors wortmannin, LY294002, LY303511, and AT1 revealed five key residues believed to be imperative for strong binding: Leu2186, Tyr2225, Ile2237, Val2240, and Ile2356. As seen in Table 5a, these residues are involved in interactions with all four ATP-competitive

mTOR inhibitors. It is important to note that none of the other six test compounds (AT2-AT7) possessed all five interactions in their LIGPLOT results, thus giving more weight to our model's accuracy. Residues Pro2169, Gly2238, and Asp2357 are of secondary importance in mTOR binding, as seen in their interaction with three of the four inhibitors, whereas residue Trp2239 has a seemingly minor contribution to binding in its interactions with only two of the four ligands.

Similarly, analysis of PI3K's interactions with crystallized ligands also revealed five residues believed to be critical for tight binding: Tyr867, Ile879, Val882, Met953, and Asp964. As seen in Table 5b, these residues take part in interactions with all five ATP-competitive PI3K inhibitors. Residues Lys833 and Ile963 contribute to a lesser degree in their contacts with four out of the five ligands, while residues Met804, Trp812, and Ile831 play a seemingly minor role in PI3K's binding behavior.

Understandably, several of these binding-relevant residues are conserved between mTOR and PI3K. Local sequence alignment shows that mTOR's Tyr2225, Ile2237, Val2240, Ile2356, and Asp2357 correspond respectively to PI3K's Tyr867, Ile879, Val882, Ile963, and Asp964 and therefore most likely play a primary role in the binding recognition of both mTOR and PI3K structures.

Selectivity

Local sequence alignment indicates several amino acid differences within the ATP-binding sites of mTOR and PI3K. In order to identify residues responsible for mTOR's specificity, LIGPLOT interactions of these unique residues within their respective

binding pockets were compared. LIGPLOT results show that residue Leu2186 participates in all of the four ligands' interactions with the protein, and, as stated above, is believed to strongly influence mTOR's ligand binding affinity. Its corresponding and unconserved PI3K residue (Ile831) plays a minor role in PI3K binding. This difference suggests that Leu2186 may be one residue of interest when designing mTOR-selective inhibitors.

Other residues unique to the mTOR active site which may play a role in specificity include Gly2238, Trp2239, and Leu2354. They are not seen in all four ligands' interactions with mTOR, but they do seem to have more importance in mTOR binding than their corresponding unconserved PI3K residues (Glu880, Ile881, and Phe961) do in PI3K binding. Interestingly, Leu2354 in particular is the only residue found in interactions with mTOR-specific LY303511 that is not seen in interactions with any other mTOR inhibitor. Perhaps this residue's potential can be exploited in the future design of selective mTOR inhibitors. Ser2165, Lys2166, and Gln2167 are unique to AT1 binding, nevertheless their contribution to AT1's specificity is uncertain, as cross-reactivity experiments with PI3K and other kinases have not yet been conducted. From a modeling standpoint, however, it is interesting to see that AT1 has a higher GOLD score when docked to PI3K (56.34) than when docked to mTOR (54.18); this may indicate that AT1 is an mTOR/PI3K dual inhibitor.

In addition, the discrepancy in size of the mTOR and PI3K active sites may also play a part in delineating specificity. As discussed earlier, the binding pocket for PI3K is smaller (surface area= 746.1 Å²; volume = 1240.9 Å³) than the mTOR binding site

(surface area = 1552.9 Å²; volume = 2451.3 Å³) and therefore may provide another strategy for designing mTOR-selective ligands. The substitutions of PI3K residues Met, Trp, Phe, Lys, Glu, Asp, and Phe for corresponding, less bulky mTOR residues Ile, Lys, Lys, Gly, Gly, Ser, and Leu are significant in that they may either allow easier entry into the binding region or afford the ligand more space to orient itself once docked in the pocket. If necessary, such a discrepancy in the sizes of the active sites can be explored further in the modification of AT1's chemical structure for increased selective mTOR inhibition.

Table 5: Residues involved in LIGPLOT hydrophobic interactions of inhibitors wortmannin, LY294002, LY303511, and AT1 in complex with A) mTOR model and B) PI3Kγ. “H” and “C” denote the existence of hydrogen and covalent bonds in the residue's interaction with the inhibitor.

A

Ligand	ATP	Wortmannin	LY294002	LY303511	AT1
mTOR Interacting Residues	Lys2166(H)		Pro2169	Pro2169	Ser2165
					Lys2166
					Gln2167
					Pro2169
		Leu 2186	Leu2186	Leu2186	Leu2186
		Tyr2225	Tyr2225(H)	Tyr2225(H)	Tyr2225
		Ile2237	Ile2237	Ile2237	Ile2237
		Gly2238		Gly2238(H)	Gly2238
	Trp2239	Trp2239		Trp2239	
	Val2240(H)	Val2240(H)	Val2240(H)	Val2240	Val2240
	Met2345		Met2345		
				Leu2354	
	Ile2356	Ile2356	Ile2356	Ile2356	Ile2356
	Asp2357	Asp2357	Asp2357(H)	Asp2357(H)	

B

Ligand	ATP	Wortmannin	LY294002	Myricetin	Quercetin	Staurosporine
PI3K Interacting Residues		Met804 (H) Ser806 (H)	Met804			Met 804
		Pro810				807 Pro810
	Ile831	Ile831	Trp812		Trp812	Trp812
		Lys833(H,C)		Ile831		Ile831
		Tyr867	Tyr867	Lys833(2H)	Lys833(H)	Lys833
		Ile879	Ile879	Tyr867(H)	Tyr867	Tyr867
			Glu880	Ile879	Ile879	Ile879
		Ile881	Ile881			Glu880(H)
	Val882(H)	Val882 (H)	Val882(H)	Val882(H)	Val882(H)	Val882(H)
	Asn951(H)		Thr887			
	Met953	Met953	Met953	Met953	Met953	Met953
			Phe961			
	Ile963	Ile963	Ile963		Ile963	Ile963
		Asp964	Asp964	Asp964	Asp964	Asp964

Inhibitor Binding Orientation

Studying the binding orientation of ligands in complex with their protein target is critical to understanding the nature of their interaction. Only in certain orientations are key ligand features able to come in close enough proximity with particular regions of the binding pocket to form hydrogen bonds and hydrophobic interactions. In our previous discussion of binding affinity and selectivity, we identified the number and type of interactions seen in mTOR's binding with ATP, wortmannin, LY294002, LY303511, and AT1. Only in analyzing the compounds' binding orientations, however, are we able to explain how the positioning of specific atoms and substructures facilitate the formation of these interactions. The conformations of

inhibitors inside the mTOR binding site can provide great insights into designing strong selective inhibitors for mTOR. Inspection of ATP, wortmannin, LY294002, LY303511, and AT1 binding poses as they appear in complex with our model structure's ATP-binding pocket reveal four protein regions potentially important for binding.

Region 1 includes residue Val2240. Val2240 forms a hydrogen bond with ATP, wortmannin, and LY294002, as well as a hydrophobic interaction with LY303511.

Region 2 consists of residues Tyr65, Ile2356, and Asp2357. Tyr65 forms hydrophobic interactions with wortmannin, LY294002, and AT1, and a hydrogen bond with LY303511. ATP and wortmannin form hydrophobic interactions with Ile2356 and Asp2357, while LY294002 and LY303511 both form hydrogen bonds with Asp2357 and hydrophobic interactions with Ile2356. **Region 3** is comprised of residues Leu2186 and Ile2237. Wortmannin, LY294002, and LY303511 all form hydrophobic with Leu2186 and Ile2237. No hydrogen bond formation has been observed in this region. **Region 4** consists of Ser2165, Lys2166, Gln2167, and Pro2169. This fourth region appears to surround the volume occupied by ATP's triphosphate chain, as one of the phosphates forms a hydrogen bond with Lys2166. AT1 forms hydrophobic interactions with Ser2165, Lys2166, Gln2167, and Pro2169. LY294002 and LY303511 form hydrophobic interactions with Pro2169.

As shown in Fig 16.d, AT1's binding orientation is compatible with the four binding regions. Although AT1 does not form hydrogen bonds with the interior of the active site, it does make hydrophobic contacts with all binding-relevant protein residues.

Fig. 16 A: Detailed view of ATP docked within mTOR binding site. ATP is displayed in ball and stick and colored by atom-type, while mTOR residues are displayed in line and colored by atom-type. Hydrogen bonds between ATP and the protein are shown in green.

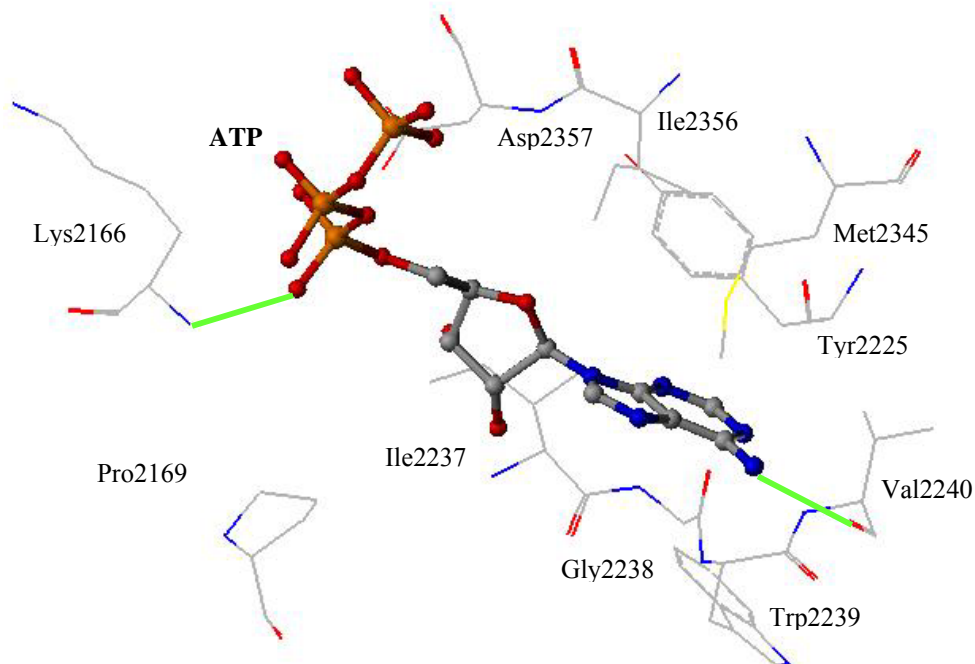


Fig. 16 B: Wortmannin docked within ATP-binding site. Wortmannin is displayed in ball and stick and colored by atom-type, while mTOR residues are shown in line and colored by atom-type. Hydrogen bonds between the ligand and the protein are shown in green.

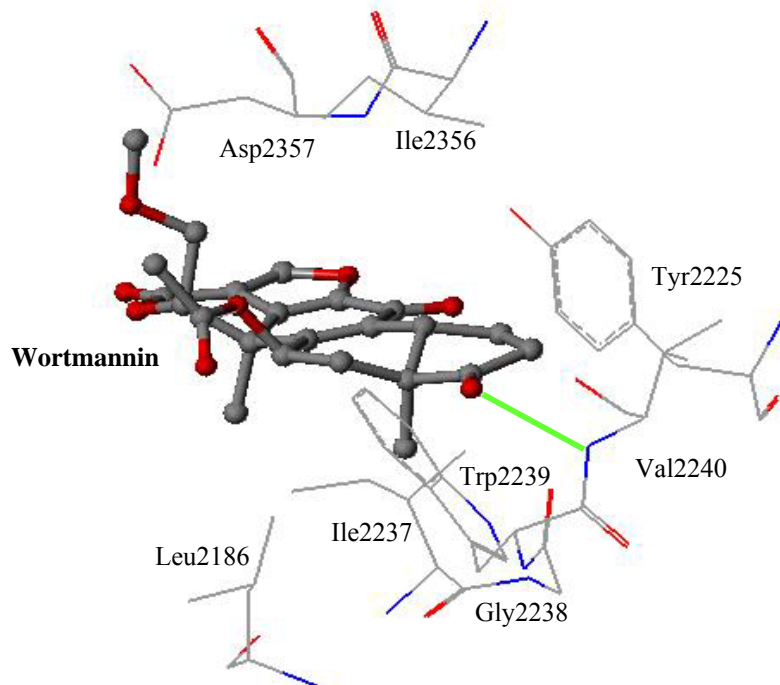


Fig. 16.c: LY294002 docked within mTOR ATP-binding site. LY294002 is displayed in ball and stick and colored by atom-type, while mTOR residues are displayed in line and colored by atom-type. Hydrogen bonds between the ligand and the protein are shown in green.

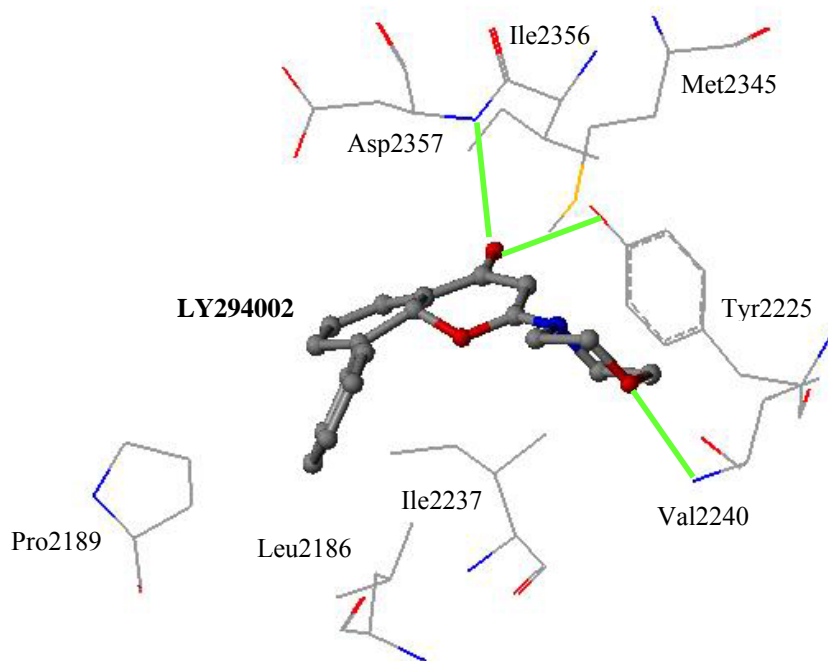
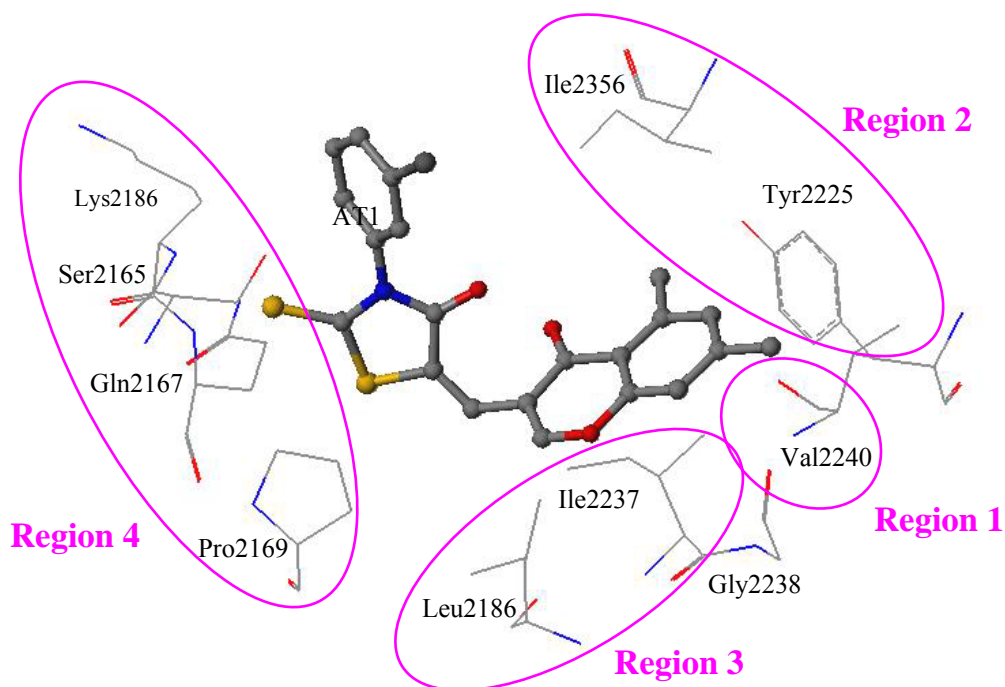


Fig. 16.d: AT1 docked within mTOR ATP-binding site. AT1 is displayed in ball and stick and colored by atom-type, while mTOR residues are displayed in line and colored by atom-type.



By superimposing the docked orientations of the inhibitors, we were able to compare bound orientations and identify common structural features among the ligands. The docked poses of ATP, wortmannin, LY294002, and AT1 are shown in Fig. 16, where features involved in the hydrogen bonding of both compounds with mTOR are encircled in green. When superimposed, ATP and wortmannin share one feature in common; they both form hydrogen bonds with Val2240 in Region 1. None of their rings overlap, as they appear to fill the active site space differently. Again, wortmannin and LY294002 both form hydrogen bonds with Val2240 in Region 1. In addition, three of their rings overlap. ATP and LY294002 share one acceptor atom feature, which forms suggests that AT1 adopts a bent conformation similar to that of ATP, where AT1's fused ring system is aligned with the length of the ATP triphosphate chain. Although they don't share any hydrogen bond interactions, it is clear that they fill the active site space similarly.

From our binding orientation analysis, we can conclude that the formation of hydrogen bonds with Val2240 in Region 1 is critical to inhibition. This was observed in all compounds with the exception of AT1, where extensive hydrophobic interactions with Region 4 compensated for its lack of hydrogen bonds with mTOR. Perhaps AT1's bent conformation allowed for close proximity to Region 4 residues and as a result, strengthened its binding. The conservation of this Val2240 hydrogen bonding pattern was expected, as it is seen in PI3K binding with ATP, wortmannin, LY294002, myricetin, quercetin, and staurosporine.

Fig. 17.a: Superimposed docked poses of ATP and wortmannin within mTOR ATP-binding site. Both compounds displayed in stick and colored by atom-type. Green circles surround atoms involved in hydrogen bonds with protein active site.

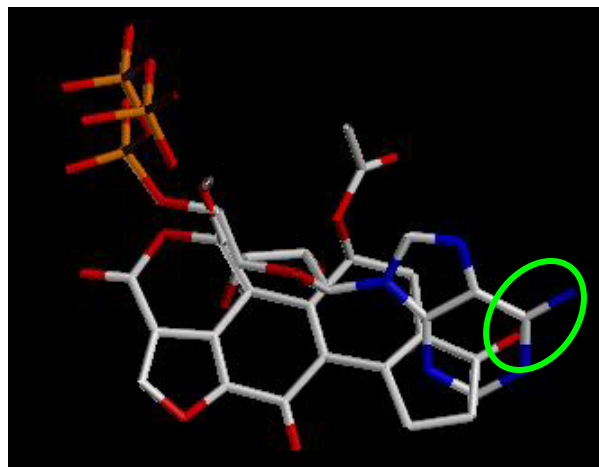


Fig. 17.b: Superimposed docked poses of wortmannin and LY294002 within mTOR ATP-binding site. Both compounds displayed in stick and colored by atom-type. Green circles surround atoms involved in hydrogen bonds with protein active site.

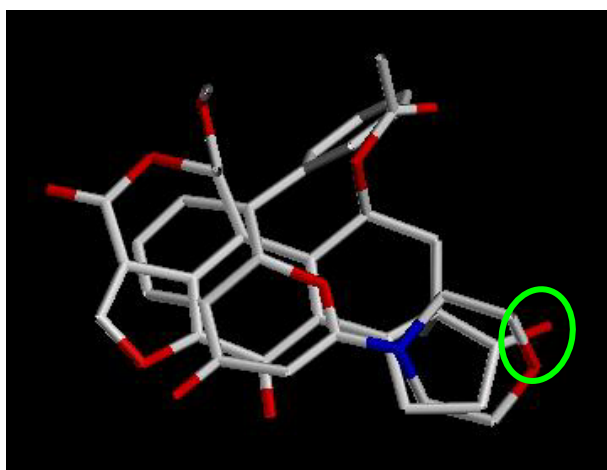


Fig. 17.c: Superimposed docked poses of ATP and LY294002 within mTOR ATP-binding site. Both compounds displayed in stick and colored by atom-type. Green circles surround atoms involved in hydrogen bonds with protein active site.

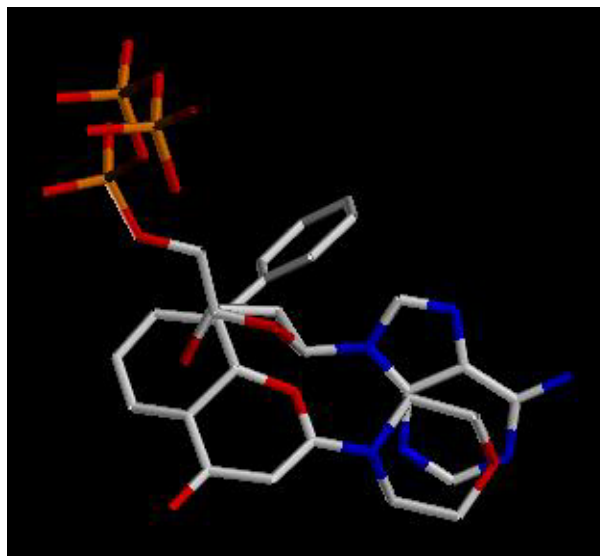
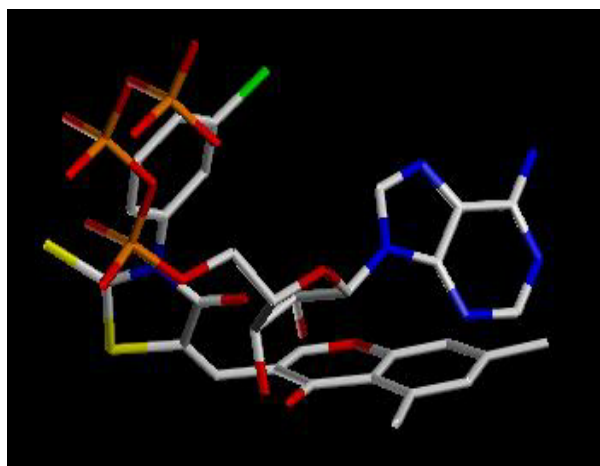


Fig. 17.d: Superimposed docked poses of ATP and AT1 within mTOR ATP-binding site. Both compounds displayed in stick and colored by atom-type. Green circles surround atoms involved in hydrogen bonds with protein active site.



SUMMARY AND CONCLUSIONS

In this study, a 3D structural model of mTOR's kinase-domain was constructed using homology modeling techniques and later refined by energy minimization and molecular dynamics simulations. Evaluation of the model structure with PROCHECK and WHATIF confirmed the successful development and validation of the 3D kinase domain. Structure and ligand-based *in silico* virtual screening techniques were used to screen commercially available small-molecule databases for potential mTOR inhibitors. The compounds retrieved from the search were analyzed and screened further using different criteria, including GOLD dockings into the 3D mTOR model, GOLD score re-ranking, Lipinski's modified rule of five, and other drug-likeness properties. Subsequent to screening, seven compounds were purchased from Maybridge and biologically tested for their ability to inhibit mTOR activity. Western blot assays show that one of the seven compounds demonstrated *in vitro* inhibitory activity on mTOR at 10 μ M concentration. The binding orientation of our hit compound (AT1) within the binding site was analyzed to identify specific mTOR residues responsible for ligand binding affinity and selectivity. Analysis of the model's interactions with docked inhibitors revealed five key residues believed to be imperative for strong binding: Leu2186, Tyr2225, Ile2237, Val2240, and Ile2356. Residue Leu2186 participates in inhibitor interactions with the protein and is believed to strongly influence mTOR's ligand binding affinity. Its corresponding and unconserved PI3K residue (Ile831) plays a minor role in PI3K binding, which suggests that Leu2186 may be one residue of interest when designing mTOR-selective inhibitors. Interestingly, Leu2354 is the only residue found in interactions with mTOR-specific LY303511 that is not seen in interactions with any other mTOR inhibitor. Perhaps this

residue's potential can be exploited in the future design of selective mTOR inhibitors, as cross-reactivity with other proteins can lead to harmful side-effects and should be avoided. Although selectivity experiments have yet to be performed for AT1, the compound's GOLD score when docked to PI3K was slightly higher than when docked to mTOR; this may indicate that AT1 is an mTOR/PI3K dual inhibitor.

CHAPTER II:

THE USE OF WORTMANNIN
PHARMACOPHORE IN
DISCOVERY OF NOVEL mTOR
INHIBITORS AT8, AT9, and AT10

MATERIALS AND METHODS

Following the successful discovery of mTOR inhibitor AT1, we decided to repeat our search for bioactive compounds with a second pharmacophore based on wortmannin's structure. Our aim was to expand our search for small molecules structurally and electrostatically compatible with mTOR's active site and in doing so retrieve more potential inhibitors with diverse structural features. Using the same mTOR kinase domain homology model constructed in Chapter 1, we altered only the pharmacophore used in our virtual search of the Maybridge database.

Virtual Screening

The same virtual screening (VS) techniques employed in Chapter 1 were repeated to screen the Maybridge database for potential mTOR inhibitors. Compounds were analyzed and screened using different criteria, including drug-likeness properties and GOLD score. Our *in silico* structure-based design strategy consisted of the following four steps:

- i) Design a wortmannin-based pharmacophore model
- ii) Perform a UNITY search of Maybridge compounds
- iii) Use modified Lipinski rules to screen search results
- iv) Dock compounds with GOLD and rank them according to their GOLD score.

Biological Assays

Cell Culture

The human HeLa cervical adenocarcinoma cell line was kindly supplied by Dr. X. F. Steven Zheng of the University of Medicine and Dentistry of New Jersey (Piscataway, New Jersey). HeLa was grown in DMEM, supplemented with 10% fetal bovine serum, 100 units/ml penicillin, and 100 mg/ml streptomycin. Cells were grown to ~60% confluence in 100 mm diameter dishes and maintained in a humidifier incubator at 37° C with 5% CO₂. Cell monolayers were washed in PBS (pH 7.4), scraped into 15-ml conical tubes, and centrifuged at 2500 rpm at 4° C for 5 min. Cell extracts were prepared by homogenizing cell pellets in ice-cold homogenization buffer. The lysates were centrifuged at 13,000 rpm at 4° C for 10 minutes. Protein concentration of the supernatants was determined according to the method of Bradford using a Bio-Rad protein assay kit (Bio-Rad Laboratories, Richmond, CA).

Western Blots

Twenty-five micrograms of cell protein extracts was resolved in 7% SDS-PAGE and transferred to PVDF membrane. Membranes were blocked for 1 hour at room temperature with 5% nonfat dry milk in TBST with 1% Tween 20. Because S6K's Thr-389 phosphorylation site is mTOR-specific [90], membranes were then incubated overnight at 4° C with Phospho-p70 S6 Kinase (Thr389) primary antibody, as well as p70 S6 Kinase primary antibody (1:1000 dilution in 5% milk/TBST, Cell Signaling Technology, Beverly MA). Following primary incubation, blots were probed with anti-rabbit polyclonal secondary antibody (1:5000 dilution in 5% milk/TBST, Cell Signaling, Beverly MA) the next morning for 1 hour at room temperature before exposing to

Western Lightning Western Blot Chemiluminescence Reagent *Plus* (PerkinElmer) per manufacturer's instructions. Blots were scanned by Hewlett Packard Scan Jet and the intensity of protein bands was quantified by ImageJ software.

RESULTS AND DISCUSSION

Pharmacophore Model

As previously explained in Chapter 1, a pharmacophore is the spatial pattern of common structural features (H-bond acceptors/donors, hydrophobic regions, etc.) that are deemed essential for protein recognition and tight binding. In order to prevent any possible covalent bond formation between mTOR and our compounds, we used the chemical structure of wortmannin, minus its furan ring, as our guide in the design of our second pharmacophore. Our pharmacophore (Fig. 17) contains two spherical hydrophobic regions (2.9 Å diameter) and three atom acceptor regions (1.2 Å diameter). Distances between features are listed in Table 6. A UNITY search of over 60,000 commercially available Maybridge compounds was then performed with this pharmacophore using Sybyl7.1.

Fig. 18. Pharmacophore inspired by the key structural elements in mTOR inhibitor wortmannin. Hydrophobic regions and acceptor atoms are represented as red and yellow spheres, respectively.

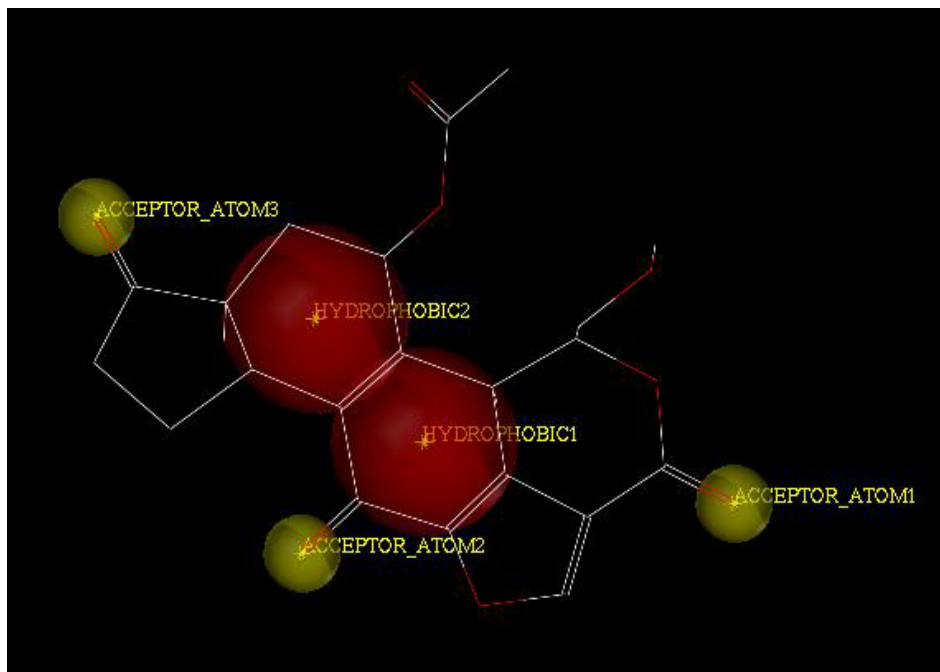


Table 6. Distances (in Angstroms) between pharmacophore features. Centroid coordinates of spheres and rings were used in calculations.

Pharmacophore Feature	Hydrophobic Sphere 1	Hydrophobic Sphere 2	Acceptor Atom 1	Acceptor Atom 2
Hydrophobic Sphere 2	2.524			
Acceptor Atom 1	4.88	7.034		
Acceptor Atom 2	2.667	3.725	6.816	
Acceptor Atom 3	6.112	3.715	10.744	6.134

UNITY Search of mTOR inhibitors

Employing our wortmannin-inspired pharmacophore as a query, we computer searched our database of over 60,000 commercially available Maybridge compounds for matches. 121 compounds satisfying the pharmacophore's structural criteria were retrieved and their 2D representations were converted into 3D structures by EM. This was performed using the Tripos force field implemented in Sybyl7.1 via the Powell minimization method with simplex initial optimization and a termination gradient of 0.05kcal/(mol*Å). The number of max iterations was set to 100 with a NB cutoff = 8.0, and a distance dependent dielectric function was used with 1.0 dielectric constant. The 121 energy-minimized compounds were then subjected to Lipinski's modified rule of five.

Lipinski's Modified Rule of Five

Lipinski's rule of five is a series of features commonly found in orally active drugs [100]. From the Maybridge database, the wortmannin pharmacophore search yielded 121 compounds, which were then filtered down in number through the use of Lipinski's "rule of 5" (shown below in bold) and other drug-likeness criteria [100]:

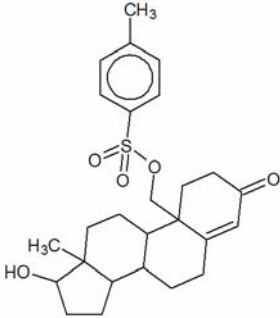
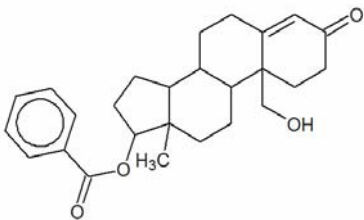
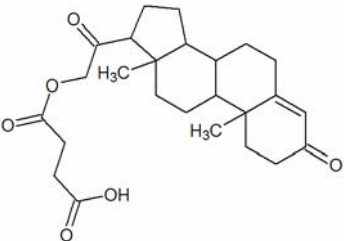
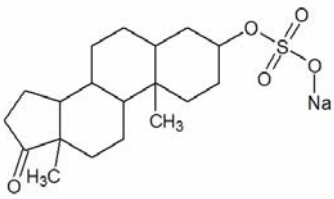
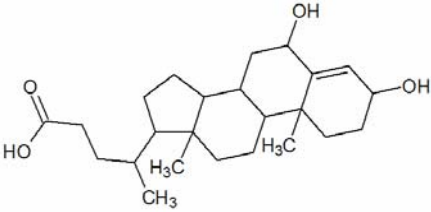
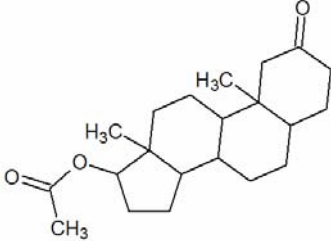
- 1) **Molecular weight < 500**
- 2) **CLogP < 5**
- 3) **Hydrogen bond acceptors > 10**
- 4) **Hydrogen bond donors < 5**
- 5) Rotatable bonds < 10
- 6) Rotatable Nitrogens < 10

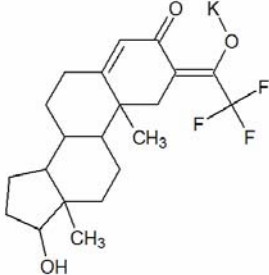
Specifically, compounds were discarded if their molecular weight > 500, their clogP > 5.0, their Hbond donors > 5, their Hbond acceptors > 10, their rotatable bonds > 10, or their rotatable Nitrogens > 10.

GOLD Docking

Those compounds satisfying Lipinski's modified rule of 5 were then docked to our homology model with GOLD (see Chapter 1 for parameter details). The compounds' GOLD scores were calculated, the docked orientations were resorted based on GOLD score instead of GOLD fitness, and the top-ranking seven compounds predicted to have the highest binding affinity for mTOR were selected for further biological evaluation. The Maybridge identification numbers of the seven compounds NRB_03664, NRB_03670, NRB_03870, NRB_03885, SB_01794, NRB_03692, and NRB_03669 were renamed AT8-AT14 for convenience. The chemical structures and GOLD scores of the seven test compounds are shown in Table 7.

Table 7. Names, chemical structures, and GOLD scores of the 7 Maybridge test compounds retrieved from pharmacophore-based UNITY search.

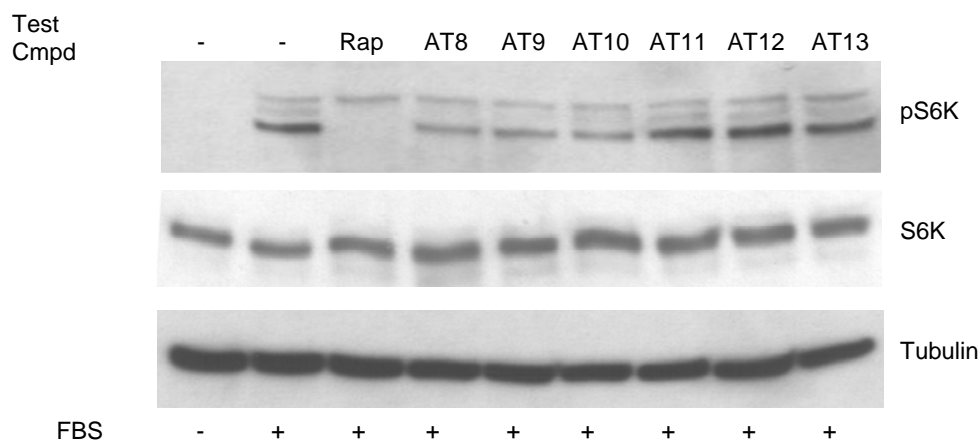
Name	Structure	mTOR GOLD score
NRB_03664 (AT8)		58.75
NRB_03670 (AT9)		52.76
NRB_03870 (AT10)		52.76
NRB_03885 (AT11)		52.28
SB_01794 (AT12)		50.85
NRB_03692 (AT13)		50.33

NRB_03669 (AT14)		50.29
------------------	---	-------

Biological Assays

For the validation of our model and its contribution to our search for novel inhibitors, Western blot experiments were used for the screening of our seven top-ranking compounds AT8-AT14 obtained by *in silico* VS. The seven compounds were purchased from the Maybridge and their inhibitory activity on mTOR was biologically evaluated in collaboration with Dr. X. F. Steven Zheng's laboratory (UMDNJ). Experimental results show that the three compounds predicted to have the highest binding affinity for mTOR, AT8, AT9, and AT10 do indeed inhibit mTOR at 10 uM concentration when compared to the rapamycin (Rap) control (Fig 18.). Results were reported as the collection of three independent experiments in duplicate. Like the inhibitor discovered in Chapter 1 (AT1), these three compounds represent potential drug candidates for a wide range of pharmacological applications including therapeutic agents for treatment of cancer, cardiovascular disease, autoimmunity, and metabolic disorders. Experimental IC₅₀ and selectivity studies for AT8, AT9, and AT10 are currently underway.

Fig. 19: Effects of rapamycin and AT8-AT13 on phosphorylation of mTOR substrate S6Kinase. Data for AT14 not shown. HeLa cells were treated with rapamycin for 30 min and AT8-AT13 for 2hrs. Cell extracts were prepared and run by 7.5% SDS-PAGE, followed by Western blot analysis using anti-pS6Kinase, anti-S6Kinase, and anti-Tubulin antibodies. Representative of three experiments.



Docking Simulation Analysis

Once AT8, AT9, and AT10's inhibition of mTOR was confirmed *in vitro*, their GOLD docking results from the prior virtual screening were revisited for a more thorough analysis of its binding interactions inside the binding pocket of the mTOR kinase active site. Our primary objective was to examine mTOR's interaction with AT8, AT9, and AT10, and in doing so identify residues responsible for binding, glean insights regarding selectivity, and increase our understanding of inhibitor orientations when bound to the active site.

The requisites and nuances of mTOR binding cannot be fully understood simply from the analysis of AT8, AT9, and AT10's interaction with the binding pocket. Therefore, the protein's interface with other known inhibitors was also explored. As a means of comparison, the binding behavior of PI3K's crystallized complexes was investigated as well. LIGPLOT diagrams were created as two dimensional representations of mTOR's

active site in complex with ATP, wortmannin, LY294002, LY303511, and AT8, AT9, AT10, as well as PI3K's active site in complex with ATP, wortmannin, LY294002, quercetin, myricetin, and staurosporine.

Binding affinity

Analysis of the mTOR model's interactions with docked inhibitors wortmannin, LY294002, LY303511, AT8, AT9, and AT10 revealed four key residues believed to be imperative for strong binding: Leu2186, Ile2237, Ile2356, and Asp2357. As seen in Table X, these residues are involved in interactions with all six ATP-competitive mTOR inhibitors. In addition, Lys2166 also has hydrophobic interactions with AT8, AT9, and AT10. It is important to note that none of the other 4 test compounds (AT11-AT14) possessed all 5 interactions in their LIGPLOT results, thus giving further credence to our model's accuracy in its structure-based prediction of inhibitors. Residues Tyr2225, Trp2239, and Val2240 are of secondary importance in mTOR binding, as seen in their interaction with four to five of the six inhibitors, whereas residues Pro2169, Met2345, and Leu2354 have a seemingly minor contribution to binding in its interactions with only three of the six ligands.

As discussed in the previous chapter, analysis of PI3K's interactions with crystallized ligands revealed five residues believed to be critical for tight binding: Tyr867, Ile879, Val882, Met953, and Asp964. As seen in Table X, these residues take part in interactions with all five ATP-competitive PI3K inhibitors. Residues Lys833 and Ile963 contribute to

a lesser degree in their contacts with four out of the five ligands, while residues Met804, Trp812, and Ile831 play a seemingly minor role in PI3K's binding behavior.

Understandably, several of these binding-relevant residues are conserved between mTOR and PI3K. Local sequence alignment shows that mTOR's Ile2237, Ile2356, and Asp2357 correspond respectively to PI3K's Ile879, Ile963, and Asp964 and therefore most likely play a primary role in the binding recognition of both mTOR and PI3K structures.

Selectivity

Local sequence alignment indicates several amino acid differences within the ATP-binding sites of mTOR and PI3K. In order to identify residues responsible for mTOR's specificity, LIGPLOT interactions of these unique residues within their respective binding pockets were compared.

As observed in Chapter 1's results, Residue Leu2186's participation in all of the four ligands' interactions with the protein, and as stated above, is believed to strongly influence mTOR's ligand binding affinity. Its corresponding and unconserved PI3K residue (Ile831) plays a minor role in PI3K binding, which suggests that Leu2186 may contribute to mTOR's specificity and therefore may be of interest when designing selective inhibitors.

Other residues unique to the mTOR active site which may play a role in specificity include Gln2167, Trp2239, and Leu2354. They are not seen in all six ligands' interactions with mTOR, but do seem to have more importance in mTOR binding than their corresponding unconserved PI3K residues (Lys808, Ile881, and Phe961) do in PI3K binding. Interestingly, Leu2354 in particular is found in interactions with mTOR-specific

LY303511, as well as AT8 and AT9. AT8 and AT9 have high GOLD scores when docked to mTOR (58.75 and 52.76) and very low GOLD scores when docked to PI3K (6.55 and 8.27) while AT10's GOLD scores for mTOR (52.76) and PI3K (48.15) are more comparable. This suggests that according to docking analysis, AT8 and AT9 may potentially be mTOR specific while AT10 may be an mTOR/PI3K dual inhibitor. Perhaps residue Leu2354's involvement in binding can be exploited in the future design of selective mTOR inhibitors.

In addition, the discrepancy in size of the mTOR and PI3K active sites may also play a part in delineating specificity. As discussed in Chapter 1, the binding pocket for PI3K is smaller than the mTOR binding site and therefore may provide another strategy for designing mTOR-selective ligands. The substitution of larger PI3K residues for corresponding smaller mTOR residues is significant in that it potentially allows easier entry into the binding region and most likely affords the ligand more space to orient itself once docked in the pocket. If necessary, such a discrepancy in the sizes of the active sites can be explored further in the structural modification of AT8, AT9, and AT10 compounds for increased selective mTOR inhibition.

Table 8. Residues involved in LIGPLOT hydrophobic interactions of inhibitors wortmannin, LY294002, LY303511, AT8, AT9, and AT10 in complex with A) mTOR model and B) PI3Kγ. “H” and “C” denote the existence of Hydrogen and Covalent bonds in the residue’s interaction with the inhibitor.

A

Ligand	ATP	Wortmannin	LY294002	LY303511	AT8	AT9	AT10
mTOR Interacting Residues	Lys2166(H)		Pro2169 Leu2186 Tyr2225 Ile2237 Gly2238	Pro2169 Leu2186 Tyr2225(H) Ile2237 Gly2238(H)	Ser2165(H) Lys2166 Pro2169 Leu2186 Tyr2225 Ile2237	Lys2166 Gln2167 Leu2186 Tyr2225 Ile2237	Lys2166 Gln2167(H) Leu2186 Ile2237
	Trp2239 Val2240(H)	Trp2239 Val2240(H)	Val2240(H)	Trp2239 Val2240	Trp2239		Trp2239 Val2240(H) Cys2243
	Met2345		Met2345		His2277 Asn2343 Met2345 Leu2354		Met2345
	Ile2356 Asp2357	Ile2356 Asp2357	Ile2356 Asp2357(H)	Leu2354 Ile2356 Asp2357(H)	Ile2356 Asp2357	Leu2354 Ile 2356 Asp2357	Ile2356 Asp2357

B

Ligand	ATP	Wortmannin	LY294002	Myricetin	Quercetin	Staurosporine
PI3K Interacting Residues		Met804 (H) Ser806 (H)	Met804			Met 804
		Pro810	Trp812		Trp812	807 Pro810 Trp812
	Ile831	Ile831 Lys833(H,C) Tyr867 Ile879	Tyr867 Ile879 Glu880	Ile831 Lys833(2H) Tyr867(H) Ile879	Lys833(H) Tyr867 Ile879	Ile831 Lys833 Tyr867 Ile879 Glu880(H)
	Val882(H)	Ile881 Val882 (H)	Ile881 Val882(H) Thr887	Val882(H)	Val882(H)	Val882(H)
	Asn951(H) Met953	Met953	Met953 Phe961	Met953	Met953	Met953
	Ile963	Ile963 Asp964	Ile963 Asp964	Asp964	Ile963 Asp964	Ile963 Asp964

Inhibitor Binding Orientation

Studying the binding orientation of ligands in complex with their protein target is critical to understanding the nature of their interaction. Only in certain orientations are key ligand features able to come in close enough proximity with particular regions of the binding pocket to form hydrogen bonds and hydrophobic interactions. The conformations of inhibitors inside the mTOR binding site can provide great insights into designing strong selective inhibitors for mTOR. Inspection of ATP, wortmannin, LY294002, LY303511, AT8, AT9, and AT10 binding poses as they appear in complex with our model structure's ATP-binding pocket reveal three protein regions potentially important for binding.

Region A consists of residues Ile2356 and Asp2357. ATP, wortmannin, AT8, AT9, and AT10 form hydrophobic interactions with Ile2356 and Asp2357, while LY294002 and LY303511 both form hydrogen bonds with Asp2357 and hydrophobic interactions with Ile2356. **Region B** is comprised of residues Leu2186 and Ile2237. Wortmannin, LY294002, LY303511, AT8, AT9, and AT10 all form hydrophobic with Leu2186 and Ile2237. No hydrogen bond formation has been observed in this region. **Region C** consists of Ser2165, Lys2166, and Gln2167. This third region appears to frame the volume occupied by ATP's triphosphate chain, as one of the phosphates forms a hydrogen bond with Lys2166. AT8 forms a hydrogen bond with Ser2165 and a hydrophobic interaction with Lys2166. AT9 forms hydrophobic interactions with both Lys2166 and Gln2167, while AT10 forms hydrophobic contacts with Lys2166 and a hydrogen bond with Gln2167.

As shown in Fig. 19, the binding orientations of AT8, AT9, and AT10 are compatible with the three binding regions. All three compounds form either hydrogen bonds or hydrophobic contacts with binding-relevant protein residues.

Fig. 20a: Detailed view of AT8 docked within mTOR binding site. AT8 is displayed in ball and stick and colored by atom-type, while mTOR residues are displayed in line and colored by atom-type. Hydrogen bonds between AT8 and the protein are shown in green.

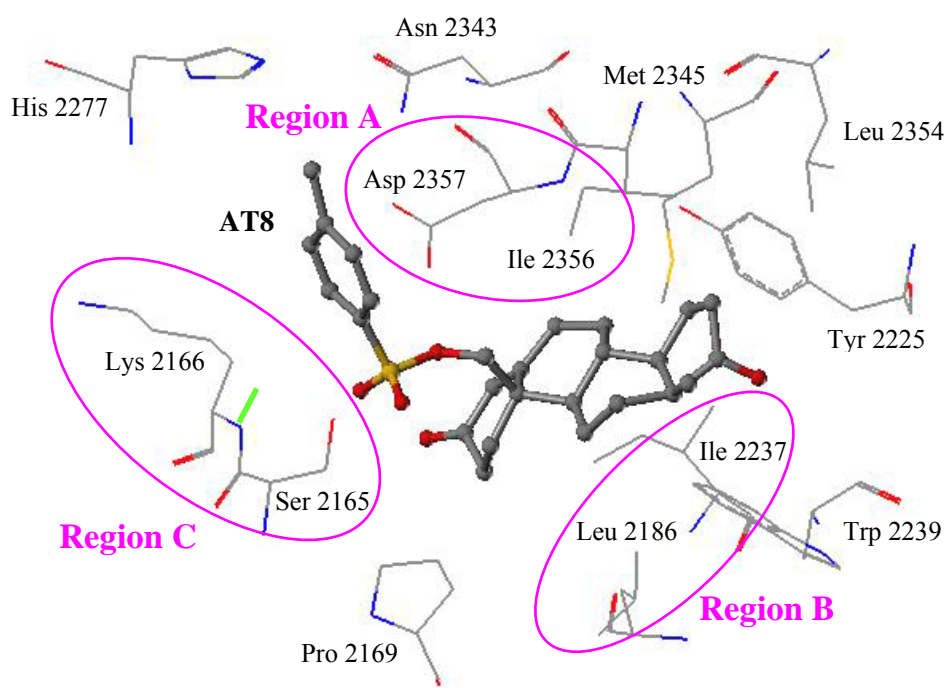


Fig. 20b: Detailed view of AT9 docked within mTOR binding site. AT9 is displayed in ball and stick and colored by atom-type, while mTOR residues are displayed in line and colored by atom-type.

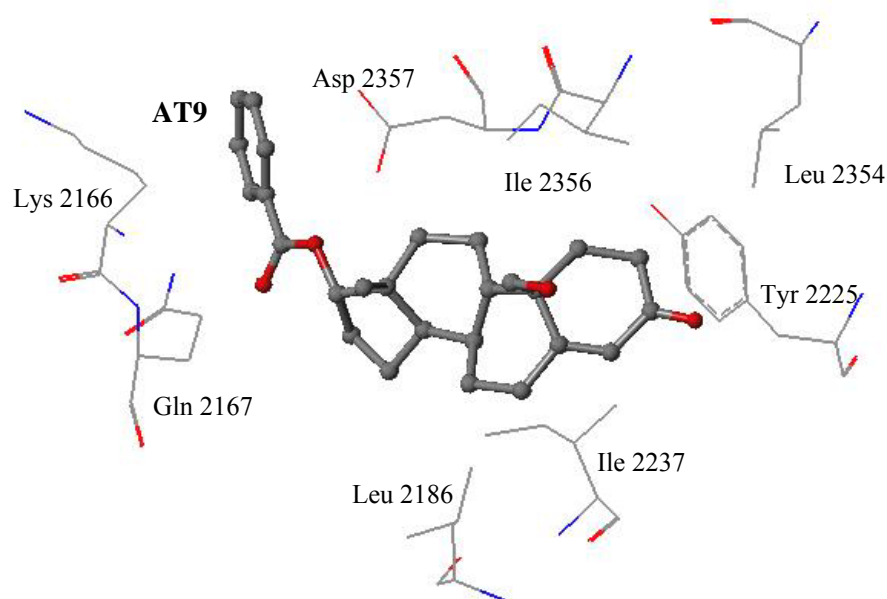
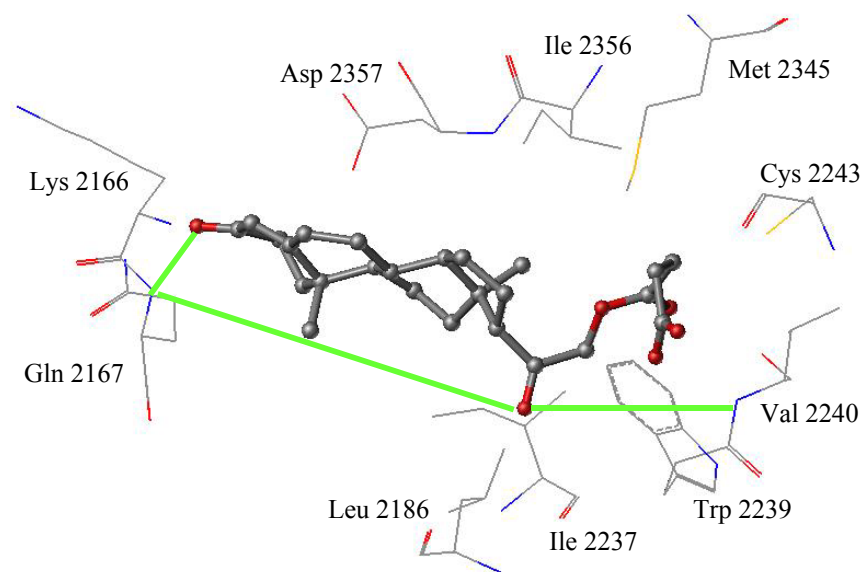


Fig. 20c: Detailed view of AT10 docked within mTOR binding site. AT10 is displayed in ball and stick and colored by atom-type, while mTOR residues are displayed in line and colored by atom-type. Hydrogen bonds between AT10 and the protein are shown in green.



The superimposition of our three inhibitors' docked conformations with ATP and wortmannin enabled us to compare their bound orientations and identify common structural features among them. The docked poses of ATP, wortmannin, AT8, AT9, and AT10 are shown in Fig. 20 where features involved in the hydrogen bonding of both compounds with mTOR are encircled in green. When superimposed, ATP and AT8 share one feature in common; they both form hydrogen bonds with residues in Region C. They also both adopt a bent, or L-shaped, conformation, where AT8's benzene ring is in line with the length ATP's triphosphate chain (Fig 20a). Three overlapping rings are seen in the superimposition of wortmannin and AT8, and it is clear from Fig. 20b that both structures' fused rings systems are docked in similar orientations. ATP and AT9 (Fig. 20c) share only one overlapping ring but appear to occupy the same space in the active site, with the exception of ATP's phosphate chain. Surprisingly, the ring systems of wortmannin and AT9 (Fig. 20d) are tilted perpendicularly to each other. AT10 does not have a bent conformation, but like ATP, still manages to form a hydrogen bond with residues in Region C (Fig. 20e). The fused rings of wortmannin and AT10 are horizontally skewed (Fig. 20f), resulting in only one overlapping ring.

From our binding orientation analysis of AT8, AT9, and AT10, we can conclude that the formation of hydrophobic contacts with residues in Regions A and B, as well as hydrogen bonds and/or hydrophobic interactions with residues in Region C, is critical to inhibition. These observations are very much in accord with our AT1 binding orientation conclusions discussed in Chapter 1. Chapter 1 binding pocket regions 2, 3, and 4 are analogous to Chapter 2 binding pocket regions A, B, and C. The one discrepancy between the two conclusions is the importance of Region 1 in binding. It appears that

compounds retrieved from the LY294002-inspired pharmacophore are more prone to form hydrogen bonds with Val2240 in Region 1, while the wortmannin-inspired pharmacophore search amassed compounds favoring interaction with Region C. Therefore, it seems that in order for a small molecule to possess mTOR inhibitory activity, it must at the very least establish interactions with Leu2186, Ile2237, and Ile2356. In addition, it must form a hydrogen bond with Val2240 or make contact with Lys2166 in Region C.

Fig. 21 a: Superimposed docked poses of ATP and AT8 within mTOR ATP-binding site. Both compounds displayed in stick and colored by atom-type. Features involved in the hydrogen bonding of both compounds with mTOR are encircled in green.

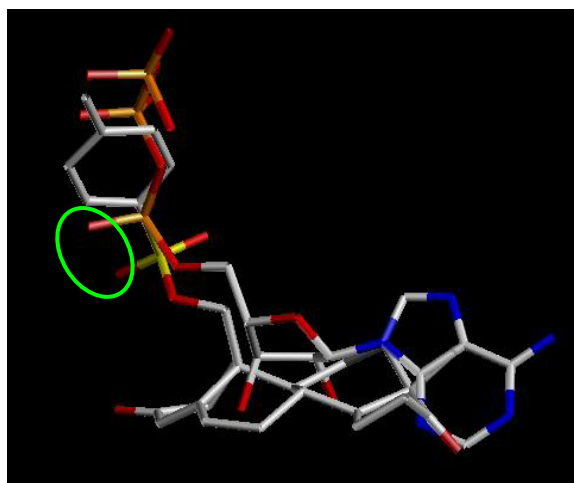


Fig. 21 b: Superimposed docked poses of wortmannin and AT8 within mTOR ATP-binding site. Both compounds displayed in stick and colored by atom-type.

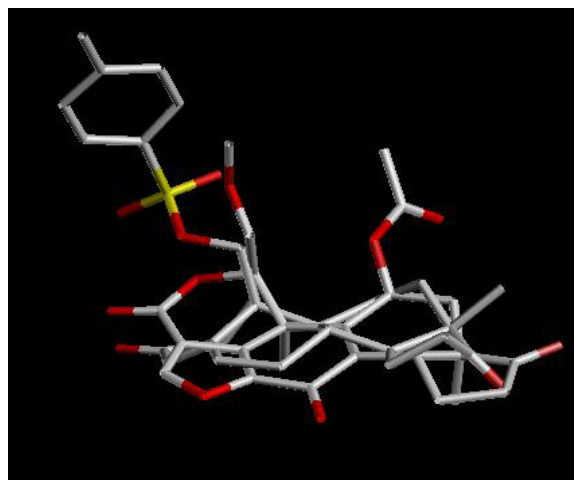


Fig. 21 c: Superimposed docked poses of ATP and AT9 within mTOR ATP-binding site. Both compounds displayed in stick and colored by atom-type.

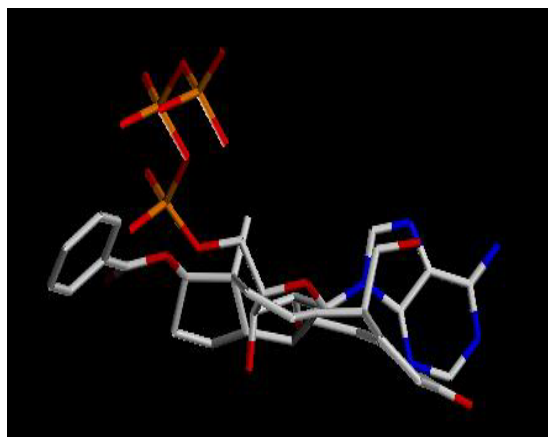


Fig. 21 d: Superimposed docked poses of wortmannin and AT9 within mTOR ATP-binding site. Both compounds displayed in stick and colored by atom-type.

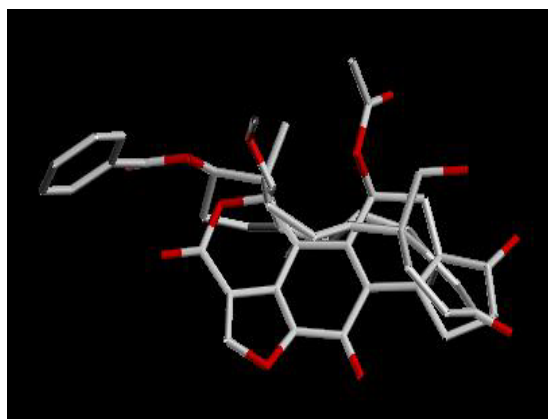


Fig. 21 e: Superimposed docked poses of ATP and AT10 within mTOR ATP-binding site. Both compounds displayed in stick and colored by atom-type. Features involved in the hydrogen bonding of both compounds with mTOR are encircled in green.

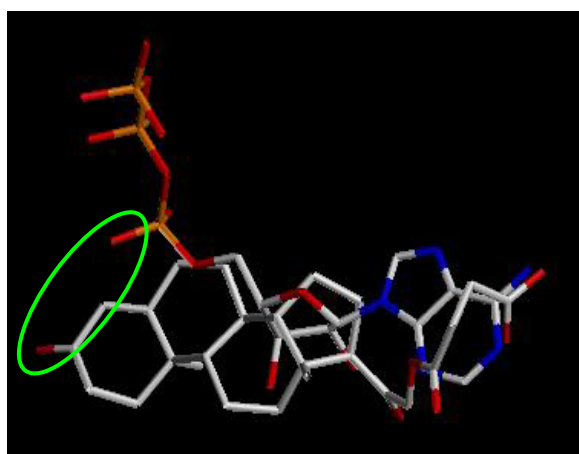
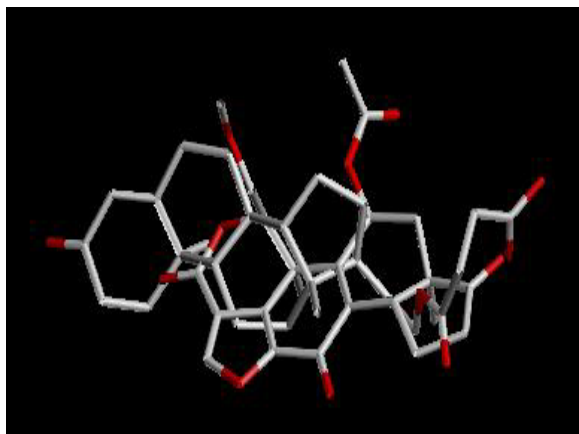


Fig. 21 f: Superimposed docked poses of wortmannin and AT10 within mTOR ATP-binding site. Both compounds displayed in stick and colored by atom-type.



SUMMARY AND CONCLUSIONS

In this second portion of the study, the same 3D structural model of mTOR constructed in Chapter 1 was utilized for the further *in silico* screening of commercially available small-molecule databases for potential mTOR inhibitors. The structurally diverse compounds retrieved from a wortmannin-inspired pharmacophore search were analyzed using different criteria, including GOLD dockings into the 3D mTOR model, GOLD score reranking, Lipinski's modified rule of five, and other drug-likeness properties. Subsequent to screening, seven compounds (AT8-AT14) were purchased from Maybridge and biologically tested for their ability to inhibit mTOR activity. Western blot assays show that three of the seven compounds demonstrated *in vitro* inhibitory activity on mTOR at 10 μ M concentration. The binding orientations of the hits (AT8, AT9, and AT10) within the binding site were analyzed to identify specific mTOR residues responsible for ligand binding affinity and selectivity. Analysis of the mTOR model's interactions with docked inhibitors revealed four key residues believed to be imperative for strong binding: Leu2186, Ile2237, Ile2356, and Asp2357.

Residue Leu2186 is believed to strongly influence mTOR's ligand binding affinity. Its corresponding and unconserved PI3K residue (Ile831) plays a minor role in PI3K binding, which suggests that Leu2186 may be one residue of interest when designing mTOR-selective inhibitors. Another residue potentially important for selectivity is Leu2354, which forms hydrophobic interactions with mTOR-specific LY303511 as well as hits AT8 and AT9. Although selectivity experiments have yet to be performed for the three compounds, AT8 and AT9 have significantly higher GOLD scores when docked to mTOR than when docked to PI3K. AT10's GOLD scores, on the other hand, are more

comparable for mTOR and PI3K. This suggests that AT8 and AT9 may potentially be mTOR-specific while AT10 may be an mTOR/PI3K dual inhibitor. Perhaps residue Leu2354's involvement in binding can be exploited in the future design of selective mTOR inhibitors.

Results from LY294002 and wortmannin pharmacophore searches and *in silico* analysis suggest that in order for a small molecule to possess mTOR inhibitory activity, it must establish interactions with Leu2186, Ile2237, and Ile2356. In addition, it must form a hydrogen bond with Val2240 or make contact with Lys2186.

FUTURE WORK

Results from the present study suggest a number of directions for future work. Our initial hits (AT1, AT8, AT9, and AT10) exhibit inhibition at 10 μ M concentration, but further IC₅₀ experiments and cross-reactivity studies are required, as their potency and selectivity have yet to be determined. Because cross-reactivity is undesirable in drug design, we need to determine whether or not our compounds inhibit other related kinases, such as PI3K. Specifically, we will test our prediction that AT8 and AT9 are mTOR-selective while AT1 and AT10 mTOR/PI3K dual inhibitors. If biological evaluation reveals any promiscuous binders, their chemical structures will be altered for the discovery of second generation compounds with increased mTOR selectivity. On the other hand, if AT1, AT8, AT9, or AT10 prove to be mTOR-specific, features in their structures responsible for facilitating interactions with binding-critical residues will be isolated and added to our LY294002 and wortmannin pharmacophores. A UNITY search of all available databases will be repeated in search of more potent inhibitors, and the resultant hits will be docked into the ATP-binding pocket of mTOR. The docking results will be filtered using the same methods described above in Chapter 1 and those small molecules emanating from the above process will be submitted to *in vitro* biological assays. Docking studies on all hit compounds will be performed to confirm or refute the contribution of residues Leu2186 and Leu2354 to mTOR selectivity.

BIBLIOGRAPHY

1. Murakami, M.; Ichisaka, T.; Maeda, M.; Oshiro, N.; Hara, K.; Edenhofer, F.; Kiyama, H.; Yonezawa, K.; Yamanaka, S. mTOR Is Essential for Growth and Proliferation in Early Mouse Embryos and Embryonic Stem Cells. *Molecular and Cellular Biology* **2004**, *24* (15), 6710-6718.
2. Sabatini, D. M.; Erdjument-Bromage, H.; Lui, M.; Tempst, P.; Snyder, S. H. RAFT1: a mammalian protein that binds to FKBP12 in a rapamycin-dependent fashion and is homologous to yeast TORs. *Cell* **1994**, *78* (1), 35-43.
3. Kim, D. H.; Sarbassov, D. D.; Ali, S. M.; Latek, R. R.; Guntur, K. V.; Erdjument-Bromage, H.; Tempst, P.; Sabatini, D. M. GbetaL, a positive regulator of the rapamycin-sensitive pathway required for the nutrient-sensitive interaction between raptor and mTOR. *Mol Cell* **2003**, *11* (4), 895-904.
4. www.wi.mit.edu/.../2003/img/ds_0429_sb.jpg
5. Wullschleger, S.; Loewith, R.; Hall, M. N. TOR signaling in growth and metabolism. *Cell* **2006**, *124* (3), 471-484.
6. Raught, B.; Gingras, A.; Sonenberg, N. The target of rapamycin (TOR) proteins. *PNAS* **2001**, *98* (13), 7037-7044.
7. www.genome.jp/kegg/pathway/hsa/hsa04150.gif
8. Ali, K.; Bilancio, A.; Thomas, M.; Pearce, W.; Gilfillan, A. M.; Tkaczyk, C.; Kuehn, N.; Gray, A.; Giddings, J.; Peskett, E.; Fox, R.; Bruce, I.; Walker, C.; Sawyer, C.; Okkenhaug, K.; Finan, P.; Vanhaesebroeck, B. Essential role for the p110delta phosphoinositide 3-kinase in the allergic response. *Nature* **2004**, *431* (7011), 1007-11.
9. Okkenhaug, K.; Bilancio, A.; Farjot, G.; Priddle, H.; Sancho, S.; Peskett, E.; Pearce, W.; Meek, S. E.; Salpekar, A.; Waterfield, M. D.; Smith, A. J.; Vanhaesebroeck, B. Impaired B and T cell antigen receptor signaling in p110delta PI 3-kinase mutant mice. *Science* **2002**, *297* (5583), 1031-1034.
10. Okkenhaug, K.; Vanhaesebroeck, B. PI3K in lymphocyte development, differentiation and activation. *Nat Rev Immunol* **2003**, *4*, 317-330.
11. Sawyer, C.; Sturge, J.; Bennett, D. C.; O'Hare, M. J.; Allen, W. E.; Bain, J.; Jones, G. E.; Vanhaesebroeck, B. Regulation of breast cancer cell chemotaxis by the phosphoinositide 3-kinase p110delta. *Cancer Res* **2003**, *63* (7), 1667-75.

12. Vanhaesebroeck, B.; Leever, S. J.; Panayotou, G.; Waterfield, M. D. Phosphoinositide 3-kinases: a conserved family of signal transducers. *Trends Biochem Sci* **1997**, *7*, 267-72.
13. Furnari, F. B.; Lin, H.; Huang, H. S.; Cavenee, W. K. Growth suppression of glioma cells by PTEN requires a functional phosphatase catalytic domain. *Proc Natl Acad Sci USA* **1997**, *94* (23), 12479-12484.
14. Rodriguez-Viciana, P.; Warne, P. H.; Dhand, R.; Vanhaesebroeck, B.; Gout, I.; Fry, M. J.; Waterfield, M. D.; Downward, J. Phosphatidylinositol-3-OH kinase as a direct target of Ras. *Nature* **1994**, *370* (6490), 527-532.
15. Rowinsky, E. K. Targeting the molecular target of rapamycin (mTOR). *Curr Opin Oncol* **2004**, *16* (6), 564-575.
16. Chan, S. Targeting the mammalian target of rapamycin (mTOR): a new approach to treating cancer. *Br J Cancer* **2004**, *91* (8), 1420-1424.
17. Long, X.; Lin, Y.; Ortiz-Vega, S.; Yonezawa, K.; Avruch, J. Rheb binds and regulates the mTOR kinase. *Curr Biol* **2005**, *15* (8), 702-13.
18. Saliman, G. A. The mammalian target of rapamycin signaling network and gene regulation. *Curr Opin Lipidol* **2005**, *16* (3), 317-323.
19. Sehgal, S. N.; Baker, H.; Vezina, C. Rapamycin (AY-22,989), a new antifungal antibiotic. II. Fermentation, isolation and characterization. *J Antibiot (Tokyo)* **1975**, *28* (10), 727-732.
20. Vezina, C.; Kudelski, A.; Sehgal, S. N. Rapamycin (AY-22,989), a new antifungal antibiotic. I. Taxonomy of the producing streptomycete and isolation of the active principle. *J Antibiot (Tokyo)* **1975**, *28* (10), 721-726.
21. Qiu, H.; Gao, R. L.; Tang, Z. R.; Meng, L.; Zhao, H.; Ruan, Y. M.; Zhao, H.; Yang, Y. J.; Chen, J. L.; Chen, Z. J. Experimental study of Mytrolimus-eluting stents on preventing restenosis in porcine coronary model. *Zhonghua Xin Xue Guan Bing Za Zhi* **2005**, *33* (6), 561-564. [Article in Chinese]
22. Dancey, J. E. mTOR inhibitors in hematologic malignancies. *Clin Adv Hematol Oncol* **2003**, *1* (7), 419-423.
23. Smolewski, P. Recent developments in targeting the mammalian target of rapamycin (mTOR) kinase pathway. *Anticancer Drugs* **2006**, *17* (5), 487-494.
24. Javier, A. F.; Bata-Csorgo, Z.; Ellis, C. N.; Kang, S.; Voorhees, J. J.; Cooper, K. D. Rapamycin (sirolimus) inhibits proliferating cell nuclear antigen expression

- and blocks cell cycle in the G1 phase in human keratinocyte stem cells. *J Clin Invest* **1997**, 99 (9), 2094-2099.
25. Franz, D. N.; Leonard, J.; Tudor, C.; Chuck, G.; Care, M.; Sethuraman, G.; Dinopoulos, A.; Thomas, G.; Crone, K. R. Rapamycin causes regression of astrocytomas in tuberous sclerosis complex. *Ann Neurol* **2006**, 59 (3), 490-498.
 26. Lloberas, N.; Cruzado, J. M.; Franquesa, M.; Herrero-Fresneda, I.; Torras, J.; Alperovich, G.; Rama, I.; Vidal, A.; Grinyo, J. M. Mammalian target of rapamycin pathway blockade slows progression of diabetic kidney disease in rats. *J Am Soc Nephrol* **2006**, 17 (5), 1395-404.
 27. Blagosklonny, M. V. Aging and immortality: quasi-programmed senescence and its pharmacologic inhibition. *Cell Cycle* **2006**, 5, (18), 2087-102.
 28. Um, S. H.; Frigerio, F.; Watanabe, M.; Picard, F.; Joaquin, M.; Sticker, M.; Fumagalli, S.; Allegrini, P. R.; Kozma, S. C.; Auwerx, J.; Thomas, G. Absence of S6K1 protects against age- and diet-induced obesity while enhancing insulin sensitivity. *Nature* **2004**, 431 (7005), 200-205.
 29. Cutler, C.; Antin, J. H. Sirolimus for GVHD prophylaxis in allogeneic stem cell transplantation. *Bone Marrow Transplant* **2004**, 34 (6), 471-476.
 30. Dumont, F. J.; Su, Q. Mechanism of action of the immunosuppressant rapamycin. *Life Sci* **1996**, 58 (5), 373-395.
 31. www.lclabs.com/PRODFILE/P-R/R-50000.JPG
 32. Brunn, G. J.; Williams, J.; Sabers, C.; Wiederrecht, G.; Lawrence, J. C. Jr; Abraham, R. T. Direct inhibition of the signaling functions of the mammalian target of rapamycin by the phosphoinositide 3-kinase inhibitors, wortmannin and LY294002. *EMBO J* **1996**, 15 (19), 5256-5267.
 33. Schultz, R. M.; Merriman, R. L.; Andis, S. L. Bonjouklian, R.; Grindey, G. B.; Rutherford, P. G.; Gallegos, A.; Massey, K.; Powis, G. In vitro and in vivo antitumor activity of the phosphatidylinositol-3-kinase inhibitor, wortmannin. *Anticancer Res* **1995**, 15 (4), 1135-9.
 34. Bondar, V.M.; Sweeney-Gotsch, B.; Andreeff, M.; Mills, G. B.; McConkey, D. J. Inhibition of the phosphatidylinositol 3'-kinase-AKT pathway induces apoptosis in pancreatic carcinoma cells in vitro and in vivo. *Mol Cancer Ther* **2002**, 1 (12), 989-97.
 35. Boehle, A. S.; Kurdow, R.; Boenicke, L.; Schniewind, B.; Faendrich, F.; Dohrmann, P.; Kalthoff, H. Wortmannin inhibits growth of human non-small-cell lung cancer in vitro and in vivo. *Langenbecks Arch Surg* **2002**, 387 (5-6), 234-9.

36. Lemke, L. E.; Paine-Murrieta, G. D.; Taylor, C. W.; Powis, G. Wortmannin inhibits the growth of mammary tumors despite the existence of a novel wortmannin-insensitive phosphatidylinositol-3-kinase. *Cancer Chemother Pharmacol* **1999**, *44* (6), 491-7.
37. Workman, P. Inhibiting the phosphoinositide 3-kinase pathway for cancer treatment. *Biochem Soc Trans* **2004**, *32* (2), 393-6.
38. Cully, M.; You, H.; Levine, A. J.; Mak, T. W. Beyond PTEN mutations: the PI3K pathway as an integrator of multiple inputs during tumorigenesis. *Nature Reviews Cancer* **2006**, *6*, 184-192.
39. Mirocha, C. J.; Abbas, H. K. Chemistry, occurrence and toxicology of the hemorrhagic mycotoxin (wortmannin) produced by *Fusarium*. *Bioact Mol* **1989**, *10*, 213-21.
40. Bosch, U.; Mirocha C. J.; Abbas, H. K.; di Menna, M. Toxicity and toxin production by *Fusarium* isolates from New Zealand. *Mycopathologia* **1989**, *108* (2), 73-79.
41. Ihle, N. T.; Williams, R.; Chow, S.; Chew, W.; Berggren, M. I.; Paine-Murrieta, G.; Minion, D. J.; Halter, R. J.; Wipf, P.; Abraham, R.; Kirkpatrick, L.; Powis, G.; Molecular pharmacology and antitumor activity of PX-866, a novel inhibitor of phosphoinositide-3-kinase signaling. *Mol Cancer Ther* **2004**, *3* (7), 763-772.
42. Davies, S. P.; Reddy, H.; Caivano, M.; Cohen, P. Specificity and mechanism of action of some commonly used protein kinase inhibitors. *Biochem J* **2000**, *351*, 95-105.
43. Fan, Q. W.; Knight, Z. A.; Goldenberg, D. D.; Yu, W.; Mostov, K. E.; Stokoe, D.; Shokat, K. M.; Weiss, W. A. A dual PI3 kinase/mTOR inhibitor reveals emergent efficacy in glioma. *Cancer Cell* **2006**, *9* (5), 341-349.
44. Walker, E. H.; Pacold, M. E.; Perisic, O.; Stephens, L.; Hawkins, P. T.; Wymann, M. P.; Williams, R. L. Structural determinants of phosphoinositide 3-kinase inhibition by wortmannin, LY294002, quercetin, myricetin, and staurosporine. *Molecular Cell* **2000**, *6* (4), 909-919.
45. Ruckle, T.; Schwarz, M. K.; Rommel, C. PI3Kgamma inhibition: towards an 'aspirin of the 21st century'? *Nat Rev Drug Discov* **2006**, *5* (11), 903-918.
46. Domin, J.; Waterfield, M. D.; Using structure to define the function of phosphoinositide 3-kinase family members. *FEBS Lett* **1997**, *410* (1), 91-95.
47. Toker, A.; Cantley, L. C.; Signalling through the lipid products of phosphoinositide-3-OH kinase. *Nature* **1997**, *387* (6634), 673-676.

48. Vanhaesebroeck, B.; Waterfield, M. D. Signaling by distinct classes of phosphoinositide 3-kinases. *Exp Cell Res* **1999**, *253* (1), 239-254.
49. Marti-Renom, M. A.; Stuart, A.; Fiser, A.; Sánchez, R.; Melo, F.; Sali, A. Comparative protein structure modeling of genes and genomes. *Annu Rev Biophys Biomol Struct* **2000**, *29*, 291-325.
50. Goldsmith-Fischman, S.; Honig, B. Structural genomics: computational methods for structure analysis. *Protein Sci* **2003**, *12* (9), 1813-1821.
51. Chung, S. Y.; Subbiah, S. The use of side-chain packing methods in modeling bacteriophage repressor and cro proteins. *Protein Sci* **1995**, *4* (11), 2300-2309.
52. Baker, D.; Sali, A. Protein structure prediction and structural genomics. *Science* **2001**, *294* (5540), 93-96.
53. Xiang, Z.; Honig, B. Extending the accuracy limits of prediction for side-chain conformations. *J Mol Biol* **2001**, *311* (2), 421-430.
54. Xiang, Z.; Soto, C. S.; Honig, B. Evaluating conformational free energies: the colony energy and its application to the problem of loop prediction. *Proc Natl Acad Sci U S A* **2002**, *99* (11), 7432-7437.
55. Petrey, D.; Xiang, Z.; Tang, C. L.; Xie, L.; Gimpelev, M.; Mitros, T.; Soto, C. S.; Goldsmith-Fischman, S.; Kernysky, A.; Schlessinger, A.; Koh, I. Y.; Alexov, E.; Honig, B. Using multiple structure alignments, fast model building, and energetic analysis in fold recognition and homology modeling. *Proteins* **2003**, *53*, 430-435.
56. Laskowski, R. A.; MacArthur, M. W.; Moss, D. S.; Thornton, J. M. PROCHECK: a program to check the stereochemical quality of protein structures. *J Appl Cryst* **1993**, *26*, 283-291.
57. Altschul, S. F.; Madden, T. L.; Schaffer, A. A.; Zhang, J.; Zhang, Z.; Miller, W.; Lipman, D. J. Gapped BLAST and PSI-BLAST: a new generation of protein database search programs. *Nucl Acids Res* **1997**, *25*, 3389-3402.
58. Thompson, J. D.; Higgins, D. G.; Gibson, T. J. CLUSTALW: improving the sensitivity of progressive multiple sequence alignment through sequence weighting, position-specific gap penalties and weight matrix choice. *Nucl Acids Res* **1994**, *22*, 4673-4680.
59. Chenna, R.; Sugawara, H.; Koike, T.; Lopez, R.; Gibson, T. J.; Higgins, D. G.; Thompson, J. D. Multiple sequence alignment with the Clustal series of programs. *Nucleic Acids Res* **2003**, *31* (13), 3497-3500.

60. Fiorentino, D. F.; Crabtree, G. R. Characterization of *Saccharomyces cerevisiae* dna2 mutants suggests a role for the helicase late in S phase. *Mol Biol Cell* **1997**, 8 (12), 2519-2537.
61. Zheng, X. F.; Fiorentino, D.; Chen, J.; Crabtree, G. R.; and Schreiber, S. L. TOR kinase domains are required for two distinct functions, only one of which is inhibited by rapamycin. *Cell* **1995** 82, 121-130.
62. Cheng, J.; Randall, A. Z.; Sweredoski, M. J.; Baldi, P.; SCRATCH: a protein structure and structural feature prediction server. *Nucleic Acids Res* **2005**, 33 (Web Server issue): W72–W76.
63. Rost, B.; Sander, C. Prediction of protein secondary structure at better than 70% accuracy. *J Mol Biol* **1993**, 232, 584–599.
64. Park, J.; Teichmann, S.A.; Hubbard, T.; Chothia, C. Intermediate sequences increase the detection of homology between sequences. *J Mol Biol* **1997**, 273, 349–354.
65. Cuff, J. A.; Clamp, M. E.; Siddiqui, A. S.; Finlay, M.; Barton, G. J. JPred: a consensus secondary structure prediction server. *Bioinformatics*, **1998**, 14 (10), 892-893.
66. Kneller, D. G.; Cohen, F. E.; Langridge, R. Improvements in Protein Secondary Structure Prediction by an Enhanced Neural Network. *J Mol Biol* **1990**, 214, 171-182.
67. Pollastri, G.; McLysaght, A. Porter: a new, accurate server for protein secondary structure prediction. *Bioinformatics* **2005**, 21 (8), 1719-1720.
68. Jones, D. T. Protein secondary structure prediction based on position specific scoring matrices. *J Mol Biol* **1999**, 292, 195–202.
69. Berman, H. M.; Westbrook, J.; Feng, Z.; Gilliland, G.; Bhat, T. N.; Weissig, H.; Shindyalov, I. N.; Bourne, P.E. The Protein Data Bank. *Nucl Acids Res* **2000**, 28, 235–242.
70. Vriend, G. WHAT IF: a molecular modeling and drug design program. *J Mol Graph* **1990**, 8, 52–56.
71. Bates, P. A.; Kelley, L. A.; MacCallum, R. M.; Sternberg, M.J.E. Enhancement of Protein Modelling by Human Intervention in Applying the Automatic Programs 3D-JIGSAW and 3D-PSSM. *Proteins: Structure, Function and Genetics* **2001**, 5, 39-46.

72. Bates, P. A.; Sternberg, M. J. E. Model Building by Comparison at CASP3: Using Expert Knowledge and Computer Automation. *Proteins: Structure, Function and Genetics* **1999**, *3*, 47-54.
73. Contreras-Moreira, B.; Bates, P. A.; Domain Fishing: a first step in protein comparative modelling. *Bioinformatics* **2002**, *18*, 1141-1142.
74. Sali, A.; Blundell, T. L. Comparative protein modelling by satisfaction of spatial restraints. *J Mol Biol* **1993**, *234*, 779-815.
75. Fiser, A.; Do, R. K.; Sali, A. Modeling of loops in protein structures. *Protein Science* **2000**, *9*, 1753-1773.
76. Guex, N.; Peitsch, M.C. SWISS-MODEL and the Swiss-PdbViewer: An environment for comparative protein modeling. *Electrophoresis* **1997**, *18*, 2714-2723.
77. Case, D. A.; Cheatham, T. E. 3rd; Darden, T.; Gohlke, H.; Luo, R.; Merz, K. M. Jr; Onufriev, A.; Simmerling, C.; Wang, B.; Woods, R. J. The Amber biomolecular simulation programs. *J Comput Chem* **2005**, *26* (16), 1668-1688.
78. Cornell, W. D.; Cieplak, P.; Bayly, C. I.; Gould, I. R.; Merz, K. M.; Ferguson, D. M.; Spellmeyer, D. C.; Fox, T.; Caldwell, J. W.; Kollman, P. A. A Second Generation Force Field for the Simulation of Proteins, Nucleic Acids, and Organic Molecules. *J Am Chem Soc* **1995**, *117*, 5179-5197.
79. Ryckaert, J. P.; Ciccotti, G.; Berendsen, H. J. C. Numerical integration of Cartesian equation of motion of a system with constraints: molecular dynamics of N-alkanes. *J Comput Phys* **1977**, *23*, 327-341.
80. Jorgensen, W. L.; Chandrasekhar, J.; Madura, J. D.; Impey, R. W.; Klein, M. L. Comparison of simple potential functions for simulating liquid water. *J Chem Phys* **1983**, *79* (2), 926-935.
81. Berendsen, H. J. C.; Postm, J. P. M.; Van Gunsteren, W. F.; Di Nola, A.; Haak, J. R. Molecular dynamics with coupling to an external bath. *J Chem Phys* **1984**, *81*, 3684-3690.
82. Morris, A. L.; MacArthur, M. W.; Hutchinson, E. G.; Thornton, J. M. Stereochemical quality of protein structure coordinates. *Proteins* **1992**, *12*, 345-364.
83. Jones, G.; Willett, P.; Glen, R. C.; Leach, A. R.; Taylor, R. Development and validation of a genetic algorithm for flexible docking. *J Mol Biol* **1997**, *267*, 727-748.

84. Verdonk, M. L.; Cole, J. C.; Hartshorn, M. J.; Murray, C. W.; Taylor, R. D. Improved protein-ligand docking using GOLD. *Proteins* **2003**, *52*, 609-623.
85. Nissink, J. W.; Murray, C.; Hartshorn, M.; Verdonk, M. L.; Cole, J. C.; Taylor, R. A new test set for validating predictions of protein-ligand interaction. *Proteins* **2002**, *49*, 457-471.
86. Kontoyianni, M.; McClellan, L. M.; Sokol, G. S. Evaluation of docking performance: comparative data on docking algorithms. *J Med Chem* **2004**, *47*, 558-565.
87. Sybyl7.1 Tripos Inc., 1699 Hanley Road, St. Louis, MO 63144.
88. Lengauer, T.; Lemmen, C.; Rarey, M.; Zimmermann, M. Novel technologies for virtual screening. *Drug Discov Today* **2004**, *9*, 27-34.
89. Muegge, I.; Enyedy, I. J. Virtual screening for kinase targets. *Curr Med Chem* **2004**, *11*, 693-707.
90. Feng, Z.; Zhang, H.; Levine, A. J.; Jin, S. The coordinate regulation of the p53 and mTOR pathways in cells. *Proc Natl Acad Sci USA* **2005**, *102* (23), 8204-8209.
91. Stan, R.; McLaughlin, M. M.; Cafferkey, R.; Johnson, R. K.; Rosenberg, M.; Livi, G. P. Interaction between FKBP12-rapamycin and TOR involves a conserved serine residue. *J Biol Chem* **1994**, *269* (51), 32027-32030.
92. Cheng, S. W.; Fryer, L. G.; Carling, D.; Sheperd, P. R. Thr2446 is a novel mammalian target of rapamycin (mTOR) phosphorylation site regulated by nutrient status. *J Biol Chem* **2004**, *279* (16), 15719-15722.
93. Takahashi, T.; Hara, K.; Inoue, H.; Kawa, Y.; Tokunaga, C.; Hidayat, S.; Yoshino, K.; Kuroda, Y.; Yonezawa, K. Carboxyl-terminal region conserved among phosphoinositide-kinase-related kinases is indispensable for mTOR function in vivo and in vitro. *Genes to Cells* **2000**, *5* (9), 765.
94. Altschul, S. F.; Gish, W.; Miller, W.; Myers, E. W.; Lipman, D. J. Basic local alignment search tool. *J Mol Biol* **1990**, *215*, 403-410.
95. Wallner, B.; Elofsson, A. All are not equal: a benchmark of different homology modeling programs. *Protein Sci* **2005**, *14* (5), 1315-1327.
96. Halgren, T. A. Merck molecular force field. I. Basis, form, scope, parameterization, and performance of MMFF94. *J Comput Chem* **1996**, *17*, 490-519.

97. Halgren, T. A. Merck molecular force field. II. MMFF94 van der Waals and electrostatic parameters for intermolecular interactions. *J Comput Chem* **1996**, *17*, 520-552.
98. Good, A. Structure-based virtual screening protocols. *Curr Opin Drug Discov Devel* **2001**, *4*, 301-307.
99. Lyne, P. D. Structure-based virtual screening: an overview. *Drug Discov Today* **2002**, *7*, 1047-1055.
100. Lipinski, C. A.; Lombardo, F.; Dominy, B. W.; Feeney, P. J. Experimental and computational approaches to estimate solubility and permeability in drug discovery and development settings. *Adv Drug Deliv Rev* **2001**, *46*, 3-26.
101. Wallace, A. C.; Laskowski, R. A.; Thornton, J. M. LIGPLOT: a program to generate schematic diagrams of protein-ligand interactions. *Protein Eng* **1995**, *8*(2), 127-134.

Curriculum Vita

Anne Theresa Tobak

- 1998-2002 **College of William and Mary**, Williamsburg, VA
Bachelor of Science, Fall 1998 – Spring 2002
Major: Computer Science
Minor: Mathematics
- 2002-2007 **Rutgers University**, New Brunswick, NJ
Doctor of Philosophy, Fall 2002 – Spring 2006
BIOMAPS Graduate Program in Quantitative Biology
Dissertation: 3D Construction of mTOR Kinase-Domain and
Discovery of Novel mTOR Inhibitors
- General Biology Teaching Assistant, Fall 2004 – Spring 2005
Life Sciences Department, Rutgers University
- Structural Bioinformatics II Instructor, Fall 2005, Fall 2006
Informatics Institute, UMDNJ